# RESEARCH ARTICLE



# Dynamics of an unusual cone-building trachyte eruption at Pu'u Wa'awa'a, Hualālai volcano, Hawai'i

Thomas Shea<sup>1</sup> • Tanis Leonhardi<sup>2</sup> • Thomas Giachetti<sup>3</sup> • Amanda Lindoo<sup>4</sup> • Jessica Larsen<sup>4</sup> • John Sinton<sup>1</sup> • Elliott Parsons<sup>5</sup>

Received: 2 June 2016 / Accepted: 14 February 2017 © Springer-Verlag Berlin Heidelberg 2017

**Abstract** The Pu'u Wa'awa'a pyroclastic cone and Pu'u Anahulu lava flow are two prominent monogenetic eruptive features assumed to result from a single eruption during the trachyte-dominated early post-shield stage of Hualālai volcano (Hawai i). Pu u Wa'awa'a is composed of complex repetitions of crudely cross-stratified units rich in dark dense clasts, which reversely grade into coarser pumice-rich units. Pyroclasts from the cone are extremely diverse texturally, ranging from glassy obsidian to vesicular scoria or pumice, in addition to fully crystalline end-members. The >100-m thick Pu'u Anahulu flow is, in contrast, entirely holocrystalline. Using field observations coupled with whole rock analyses, this study aimed to test whether the Pu'u Wa'awa'a tephra and Pu'u Anahulu lava flows originated from the same eruption, as had been previously assumed. Crystal and vesicle textures are characterized along with the volatile contents of interstitial glasses to determine the origin

Editorial responsibility: K.V. Cashman

**Electronic supplementary material** The online version of this article (doi:10.1007/s00445-017-1106-z) contains supplementary material, which is available to authorized users.

- ☐ Thomas Shea tshea@hawaii.edu
- Department of Geology and Geophysics, SOEST, University of Hawaii, Honolulu, HI 96822, USA
- Department of Earth & Planetary Science, University of California Berkeley, Berkeley, CA 94720, USA
- Department of Earth Sciences, University of Oregon, Eugene, OR 97403, USA
- Department of Geology and Geophysics, University of Alaska Fairbanks, Fairbanks, AK 99775, USA
- Division of Forestry and Wildlife, Honolulu, HI, USA

Published online: 02 March 2017

of textural variability within Pu'u Wa awa a trachytes (e.g., magma mixing vs. degassing origin). We find that (1) the two eruptions likely originated from distinct vents and magma reservoirs, despite their proximity and similar age, (2) the textural diversity of pyroclasts forming Pu'u Wa'awa'a can be fully explained by variable magma degassing and outgassing within the conduit, (3) the Pu'u Wa'awa'a cone was constructed during explosions transitional in style between violent Strombolian and Vulcanian, involving the formation of a large cone and with repeated disruption of conduit plugs, but without production of large pyroclastic density currents (PDCs), and (4) the contrasting eruption styles of Hawaiian trachytes (flow-, cone-, and PDC-forming) are probably related to differences in the outgassing capacity of the magmas prior to reaching the surface and not in intrinsic compositional or temperature properties. These results further highlight that trachytes are "kinetically faster" magmas compared to dacites or rhyolites, likely degassing and crystallizing more rapidly.

**Keywords** Trachyte · Hawai'i · Pyroclastic cone · Textural analysis · Vulcanian · Violent strombolian

# Introduction

# General context of the study

Trachyte volcanism commonly occurs at continental rifts (e.g., Chaîne des Puys, France; Kenya rift, Africa, Boivin et al. 2009; King et al. 1972), subducting arcs (e.g., Roman Province and Campanian volcanoes, Italy, Pecerillo 2005), and intraplate settings (e.g., Canary Islands, Hawai i, Freundt and Schmincke 1995; Cross 1904). Purely magmatic (i.e., no involvement of external water) trachyte eruptions



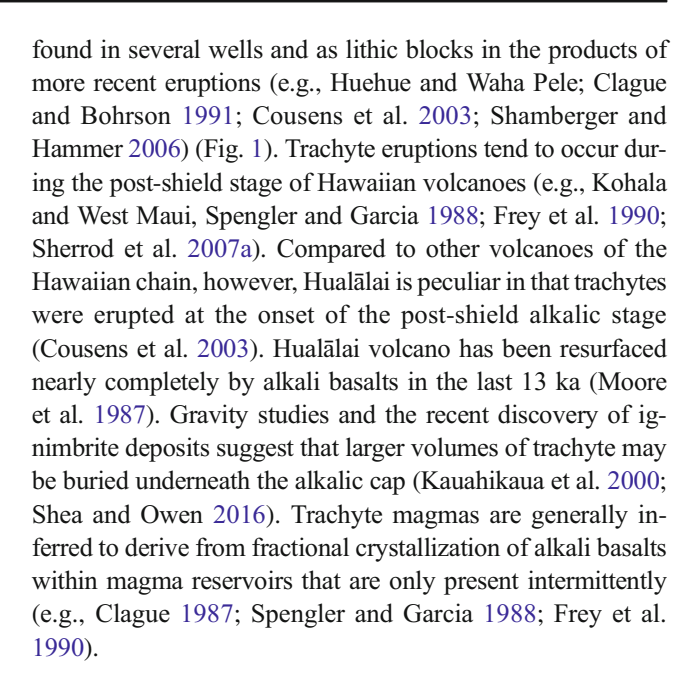
26 Page 2 of 24 Bull Volcanol (2017) 79:26

often produce domes that can be associated with pyroclastic fall deposits and density currents (Velde 1978; Závada et al. 2009; Boivin et al. 2009; Miallier et al. 2010), as well as large ignimbrite deposits (e.g., Barberi et al. 1978; Freundt and Schmincke 1995). Despite the relative paucity of field, experimental, and physical constraints on trachyte magmas compared to rhyolites, recent efforts have improved our understanding of the viscosity (Whittington et al. 2001; Giordano et al. 2004), H<sub>2</sub>O solubility and diffusivity (Di Matteo et al. 2004; Fanara et al. 2013), mineral phase relations (Fabbrizio and Carroll 2008; Martel et al. 2013), and feldspar crystallization kinetics (Arzilli and Carroll 2013) of highly alkaline melts. These studies show that trachytes differ from rhyolites in being less viscous, incorporating more dissolved water at a given pressure and crystallizing relatively rapidly. Yet only a handful of trachyte eruptions have been studied in detail in terms of eruption products and conduit dynamics (Polacci et al. 2003; D'Oriano et al. 2005; Colombier et al. 2017). As a result, we have a relatively limited understanding of this type of volcanism, particularly for eruptions involving moderate volumes of magma (i.e., <few km<sup>3</sup>). Do trachyte eruptions also display transitions between flow or dome-building activity and tephra-producing phases like their calc-alkaline counterparts? How does magma ascent and degassing efficiency in trachytes compare with calc-alkaline magmas?

In Hawai i, magmas with evolved compositions ( $SiO_2 > 60$  wt%) erupt infrequently and typically produce voluminous domes and flows (e.g., Stearns and Macdonald 1942, 1946). The Pu'u Wa'awa'a cone and Pu'u Anahulu lava flow are preserved surface expressions of intraplate trachyte volcanism thought to have occurred during the transition from shield to post-shield stage of Hualālai volcano about 92,000-114,000 years ago (Cousens et al. 2003). The close spatial association between the two, combined with their distinct eruption styles, offers in principle a unique opportunity to investigate the ascent and degassing conditions of Hawaiian trachytes and the potential causes for differing eruptive styles (e.g., explosive/effusive).

# Geological setting: trachyte volcanism along the Hawai i chain

Within the Hawaiian chain, trachytes have been identified only on the islands of Maui and Hawai i, although other types of evolved lava have also been recognized on Oahu (e.g., the Kuwale rhyodacite, Van der Zander et al. 2010). At West Maui volcano, trachytes occur as numerous bulbous domes and thick blocky lava flows distributed around the flanks (Stearns and Macdonald 1942; Velde 1978), whereas they are almost absent on East Maui. On the island of Hawai i, trachyte domes and lava flows outcrop on Kohala volcano (Stearns and Macdonald 1946; Spengler and Garcia 1988), at Hualālai (Pu'u Wa'awa'a and Pu'u Anahulu) and have been



# The Pu'u Wa'awa'a-Pu'u Anahulu trachyte association at Hualālai

Pu'u Wa'awa'a ("hill of many furrows") on the northeast flank of Hualālai volcano (Island of Hawai i) is a prominent 1.6-km-diameter, ~250–300-m-high cone (elev. 1209 m absl) that is open on the south-east side (Fig. 1a, b). The cone is completely surrounded by younger (<13 ka) Hualālai lava flows (Moore et al. 1987; Sherrod et al. 2007b) as well as alluvium/talus material eroded from the cone. Pu'u Wa'awa'a (hereafter designated as PWW) is composed of trachytic pyroclasts, including pumice and obsidian. Clague and Bohrson (1991) examined rare dunite and gabbro xenoliths enclosed within pumice clasts from PWW and found that in contrast to other olivine-bearing xenoliths from Hualālai, the xenoliths contained no CO<sub>2</sub> in melt inclusions. Instead, the presence of hydrous mineral reaction rims at the xenolithtrachyte interface suggests that the PWW trachyte magma was water rich and CO<sub>2</sub> poor.

The Pu'u Anahulu (PA) flow occurs as a series of thick (up to 260 m) blocky ridges and lobes northwest of PWW (Fig. 1a, c). Two to three thick (between 50 and 90 m) flow units can be inferred from satellite imagery and field observations. A water well drilled on the eastern end of the flows also suggests that those units are each >70 m thick (Clague and Bohrson 1991).

PWW and PA were first described as separate trachyte occurrences by Cross (1904) and subsequently inferred to have originated from the same vent by Stearns and Macdonald (1942). Moore et al. (1987) estimated the combined volume of the lava flow and cone to be about  $5.5~\rm km^3$  or the largest single eruption identified in Hawai i. Clague (1987) dated PWW at  $106~\pm~6~\rm ka$  using K-Ar, and Cousens et al. (2003)



Bull Volcanol (2017) 79:26 Page 3 of 24 26

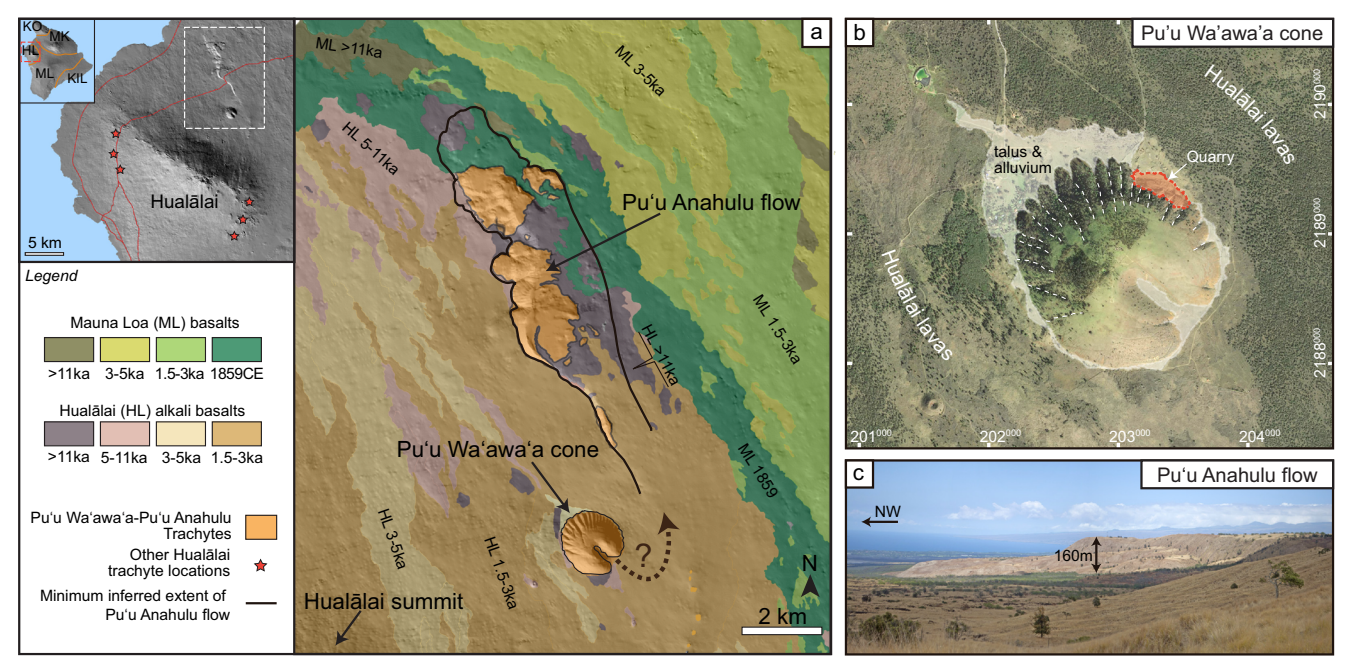


Fig. 1 a Geological map of the Pu'u Wa'awa'a-Pu'u Anahulu surroundings with ages of more recent (<13 ka) basaltic lava flows from Hualālai and Mauna Loa (modified from Shea and Owen 2016, unit boundaries from Wolfe and Morris 1996 and Sherrod et al. 2007b). *Thick orange arrow* shows the previously inferred connection between

the Pu u Wa awa a cone and the Pu u Anahulu flow. Upper left inset shows a digital elevation model of Hual $\bar{a}$ lai volcano, Hawai i, and location of study area. b Aerial photo of Pu'u Wa'awa'a cone and c side view of Pu'u Anahulu flow

obtained a similar age of  $113.5 \pm 3$  ka for PA using Ar-Ar, confirming that the two were closely related in time. Geochemical analyses also revealed that PA and PWW were only marginally distinct with respect to bulk composition and Pb isotopes (Cousens et al. 2003). Shamberger and Hammer (2006) suggested that the PWW-PA trachyte magma originated via rapid differentiation (i.e., <20 ka in duration) of large volumes of alkali basalt at 3–7 kbar during transition from shield to post-shield magmatism at Hualālai.

# Study objectives

The present study examines in detail the deposits of the PWW cone and PA flow. Although both trachyte locations are considered to have originated from the same vent during the same eruption, to date, no field relationship has confirmed this interpretation. Through a combination of field work, geochemical analyses, and textural characterization of the eruption deposits, this investigation examines the possible spatiotemporal link between the two trachyte locations and provides new constraints on magma ascent, degassing, and eruption dynamics. The principal questions we aim to answer are the following: (1) Are PWW and PA genetically related? (2) What eruption styles formed PWW? (3) How was the remarkable diversity of pyroclast textures generated? (4) Are there changes in magmatic conditions (i.e., fluctuations in magma composition, volatile contents, crystallinity, overpressure, ...) that may explain differences in the expression of trachyte volcanism in Hawai'i?

# Methods

# Field work and sampling

Field work on both PWW and PA was used to assess their potential linkage and for sample collection. The complete distribution of the PWW tephra is unknown due to the presence of overlying lava flows (cf. Fig. 1a, b). Several pits dug around the PWW cone showed that the deposits mantling the base of the cone were talus and alluvium. The presence of an old 20th C. quarry on the northern side of the cone (Fig. 1b) allowed access to tens of meters of proximal eruption deposits. While this location preserves an important record of the eruption sequence, proximal cone environments often contain deposits that were remobilized during syn-eruptive granular flow and slumping (e.g., Branney and Kokelaar 2002; Cagnoli et al. 2015). Therefore, deposits were separated into six large stratigraphic "packets" that could be followed from one location to another within the quarry, and sampling was restricted to one to three continuous units from each packet. Within the quarry, the combined thickness of the six packets is about 24 m. Between 85 and 150 pyroclasts



26 Page 4 of 24 Bull Volcanol (2017) 79:26

~1–3 cm in size were collected within each selected units using methods described in Shea et al. (2010a). As clast textures were highly variable even within a single bed, we attempted to avoid biased sampling (e.g., pumice over obsidian) by iteratively picking the closest next lapilli clast with a size >0.5 cm located laterally in the bed. A total of 11 units were sampled in this fashion within the six main packets defined.

PA samples were collected in both the most proximal and distal areas. Since the blocky lava flow surface is significantly altered, large blocks and boulders were usually broken up until ~10–20-cm pieces of the unaltered interior could be sampled. In the more distal regions of the flow, deep gullies allow access to fresh rock exposures. Nine samples were selected for bulk chemistry and thin sections.

### Density/vesicularity measurements

Pyroclast densities were measured using the Archimedes method (e.g., Shea et al. 2010a). Briefly, clasts were cleaned, sonified, dried, numbered by size, and weighed. Clasts were then wrapped in wax paper and weighed again under water to derive density. Two billets were cut from holocrystalline and obsidian samples and weighed in the same fashion to obtain bulk rock density for the trachyte (average ~2400 kg m<sup>-3</sup>). These billets were verified to be vesicle free by examining associated thin sections. The vesicle-free trachyte density was then used to calculate vesicularity for each clast. Each clast was also categorized by its textural appearance in hand sample as "pumiceous," "scoriaceous," "cryptocrystalline," "obsidian," or "microbreccia." Thin sections were made for 5-7 clasts spanning the range of density/vesicularity distributions for each of the 11 sampled units.

# **Bulk rock chemistry**

The 9 PA flow samples and 12 of the largest PWW clasts were crushed for X-ray fluorescence (XRF) analyses. Prior to crushing, the superficial 1–3 cm of each sample was removed using a precision saw to discard potential alteration fronts. Resulting slabs/billets were then crushed using a tungsten carbide-plated hydraulic rock splitter, sonified, dried, and powdered using an alumina mill. Approximately 10–20 mg of each powdered sample was used to prepare fused disks for analyses, carried out using a Siemens 303AS fully automated, wavelength dispersive XRF at the University of Hawai'i. Details on standard calibration and reproducibility can be found in Sinton et al. (2005), and the data are reported in Table A1 (Supplementary Material).



Glass and mineral (chiefly feldspar) analyses were conducted using a JEOL-8500F field-emission gun Hyperprobe at the University of HawaiHawai'i. Spot analyses of glasses were performed using an accelerating voltage of 15 keV, a 10-nA beam current, a 6-10-µm beam diameter, and count times of 20 s (Si, Ti, Na, K, P), 30 s (Fe, Mn), and 70 s (Al, Mg, Ca, Cl). Since Si gains and Na losses can be problematic for glass analyses (e.g., Morgan and London 1996; Shea et al. 2014), we adopted the time-dependent intensity method (i.e., where intensities are compared at 5-s intervals) incorporated within the Probe for EPMA software to correct for this problem. Four to five spots were acquired for each glass analyzed, with standard glasses analyzed repeatedly to monitor for analytical drift. Relative analytical precision is <1% (Si, Al), 1-3% (Fe, Mn, Mg, Ca, Na), 5% (Ti, Cl), and 15% (P). Average glass analyses are reported in Table A2 (Supplementary Material).

A similar element setup was used for feldspar analyses, except for a higher beam current of 30 nA, smaller beam diameters of 3–6  $\mu$ m, and longer counting times of 30 s for Si, Ti, Na, K, and P. Mineral standards were used for calibration and to monitor drift, and analytical precision is similar to that of glass analyses.

### Phase abundance

Images acquired at the electron microprobe were used to determine glass, vesicle, and feldspar abundances within samples analyzed for chemical composition. Manual thresholding and outlining of the feldspars ensured that phases could be well distinguished within grayscale images. The areas of each phase (glass, vesicles, and feldspar) were divided by the image areas to determine phase proportions.

# Volatile analyses

Volatiles ( $H_2O$  and  $CO_2$ ) were first analyzed within three doubly polished obsidian chips from PWW using a Thermo Scientific Nicolet 6700 Fourier transform infrared (FTIR) spectrometer with a  $20 \times 20$ - $\mu$ m aperture at the University of Alaska Fairbanks. Transmission analyses were obtained over the wavenumber range  $\nu = 6500-650~\rm cm^{-1}$ , with spectra consisting of 512 scans at a resolution of 4 cm<sup>-1</sup>. Samples were placed on a NaCl disk where background and sample analyses were acquired under the same analytical conditions. Samples were then transferred to a gold-coated mirror for reflectance measurements. The refractive index was calculated using Church and Johnson (1980) wafer thickness derived using the interference fringe technique (Nichols and Wysoczanski 2007), and a molar absorptivity of



Bull Volcanol (2017) 79:26 Page 5 of 24 26

 $66.9 \text{ L mol}^{-1} \text{ cm}^{-1}$  (Behrens and Hahn 2009) was used to calculate  $H_2O_t$  from the  $3570\text{-cm}^{-1}$  band.

Water was also measured in thin sections from the different clasts using microRaman spectroscopy (see Supplementary Table A2). The technique requires calibration standards to attain sufficient accuracy; we used the methods described in Le Losq et al. (2012) and Shea et al. (2014). Five to eight spot analyses were collected in clasts with different textures. An analytical profile was collected within one sample showing textural heterogeneity, and two additional transects and a map were acquired within one obsidian sample close to the clast edge to check for potential heterogeneity associated with rehydration rinds (cf. "rehydration in the PWW pyroclasts" in the Supplementary Material).

Thermogravimetric analyses (TGA) were also performed on a subset of samples to further evaluate the possibility of significant rehydration by meteoric water (Giachetti and Gonnermann 2013). The methodology used is described in detail by Giachetti et al. (2015) and in the Supplementary Material.

# Results and interpretations

#### Field observations

Proximal stratigraphy of PWW deposits Previous quarrying activity near the base of the PWW cone (cf. Fig. 1) exposed about 10-15 m of stratified tephra on each side of the quarry walls, typically dipping by about 20–25° (Fig. 2a, b). The base of the deposits is not exposed, and the top of the PWW sequence is overlain by a much younger (~2 ka) Hualālai lava flow (Fig. 2b). The most striking feature of the tephra sequence is the overall lack of lateral continuity between beds and the pinching and swelling nature of the contacts, making it difficult to follow a single layer further than the scale of a 10-m wide outcrop. These characteristics, combined with the lack of clear marker horizons, made defining individual stratigraphic units challenging. Field work around the proximal deposits therefore focused on defining "packets" of units that could be identified from one location to another. Despite the difficulties in correlating the finer units, a stratigraphical reconstruction was made based on two opposing quarry exposures (Fig. 3).

The topmost portion of the deposit (~2.5 m, cf. Fig. 3) consists of baked clay (formed during emplacement of an overlying ~2 ka lava flow, Fig. 2b) and altered ash overlying a series of lenticular, discontinuous thin pumice lapilli-dominated units that show clear evidence for small-scale erosion/gullying and which we interpret as post-eruptive reworking of the deposits and later soil formation. The eruptive sequence is dominated by two repeated lithofacies (Fig. 3a, b). The first is a "massive pumice/obsidian/scoria lapilli" facies (abbreviated mL here

following Branney and Kokelaar 2002) consisting of clast-supported, fairly well-sorted, and typically reverse-graded lapillidominated layers containing various proportions of pumiceous, scoriaceous, cryptocrystalline, and obsidian clasts. This facies is usually massive and more rarely faintly bedded and contains a significant proportion of blocks and bombs (up to 1.5 m in size) in some subunits (Fig. 2c). The second is a "poorly sorted, coarse ash-lapilli cross-stratified facies" (labeled "xsLT") often dominated by poorly vesicular scoria, cryptocrystalline clasts, and obsidian, with typically less pumice (Figs. 2d and 3). These units frequently include randomly scattered, dense blocks up to 50 cm of cryptocrystalline and obsidian material, most often at their base. Diffuse bedding of coarse ash and fine lapilli is common, frequently intercalated between cross-stratified thin ash beds (1–10 cm) that pinch and swell at the outcrop scale (Fig. 2d–g). The xsLT facies commonly transitions gradually to mL, whereas contacts between mL and overlying xsLT are more abrupt (Figs. 2d-g and 3).

Repeated alternations between these two facies constitute the bulk of the PWW deposits and are interpreted as fall deposits (*m*L) preceded by conduit clearing phases (*xs*LT). We infer both facies to have undergone significant downslope remobilization during deposition (i.e., syn-eruptive destabilization). The lines of evidence supporting these interpretations are discussed below.

Most of the lower units of the sequence examined (grouped into "packet 6", Fig. 3) display a light brown to reddish coarse ash matrix, with clasts that also show brick red interiors when broken. This coloring is likely associated with slow cooling and oxidation of clasts. The bottommost unit from packet 6 is dominated by oxidized welded spatter, confirming that the sequence was cooled more slowly than deposits from packets 1–5, which rarely show signs of oxidation.

No unambiguous pyroclastic density current (PDC) deposits were found within the proximal PWW cone sections. A ~2-m trachytic ignimbrite sequence was discovered nearby on top of the PA flows (the Hualālai ignimbrite HI, Shea and Owen 2016), but no PWW tephra deposits were observed above or below that unit. Either (1) the PWW fall sequence was never deposited in this area (i.e., away from dispersal axis) or (2) the fall sequence has been completely eroded from the top of the PDCs or (3) PWW tephra preceded both the PDCs and PA.

Pyroclast characteristics Pyroclasts from the proximal PWW deposits fall within a spectrum encompassing four categories: (1) "pumiceous" clasts are cream colored, lightweight, and macro- to microvesicular (Fig. 4a, b); (2) "scoriaceous" clasts are usually brown, denser, and moderately vesicular (Fig. 4c); (3) "cryptocrystalline" clasts are dark brown, dense, generally non-vesicular, and without visible glass (Fig. 4d); and (4) "obsidian" clasts are dark and glassy with conchoidal or planar surfaces (Fig. 4e). These textural end-members are rarely found



26 Page 6 of 24 Bull Volcanol (2017) 79:26

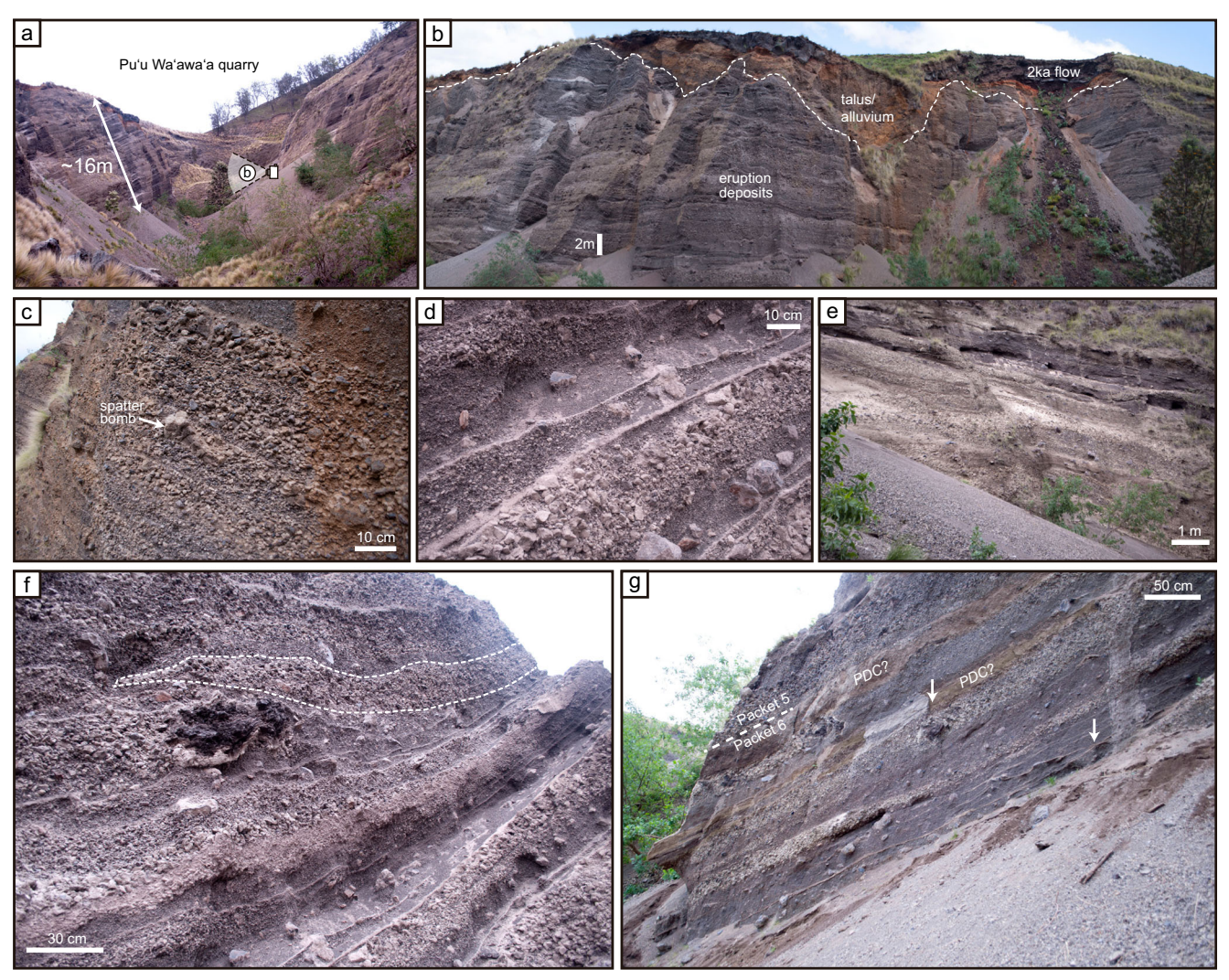


Fig. 2 a Overview of the Pu'u Wa'awa'a quarry showing the >10-m thick proximal sections exposed. b Northern section of the quarry with part of the ∼110-ka Pu'u Wa'awa'a tephra sequence overlain by alluvium and a more recent (2 ka) Hualalai basalt flow. c Close-up of massive pumice-rich lapilli-dominated units (pmL, see Fig. 3) from packet 3. Note the presence of angular darker obsidian and microcrystalline clasts and the faint inverse grading. d Two sequences from packet 2 of dark-clast-rich coarse-ash-dominated cross-stratified basal beds (soxsLT, see Fig. 3) transitioning towards coarser pumice-rich lapilli-dominated beds (pmL). The basal beds are poorly sorted compared to the pumice-rich beds and contain large, dense obsidian and cryptocrystalline lapilli and

blocks. e Near the base of units exposed within the quarry (packet 6), clasts are enclosed within a finer, more oxidized, variably indurated matrix. The bottommost unit exposed is an agglutinate of pumice and scoria enclosed within a reddish coarse ash matrix. f Multiple repetitions of cross-stratified coarse ash units reversely grading into pumice-rich lapilli units within packet 2, illustrating the pinching and swelling nature of stratification and the presence of discontinuous pumice lenses (white dotted line). Note the presence of >50 cm cow-dung bomb. g Section roughly along direction of maximum dip (26°) with units from packets 5 and 6 displaying clear duplexing (white arrows mark the start of bed separation)

pure but instead display gradual (e.g., Fig. 4f) or abrupt (Fig. 4g) transitions from one to another, as well as intricate banding and folding (Fig. 4h, i). No obvious accidental non-juvenile clasts (e.g., basalts) were found in any of the PWW deposits. Like Clague (1987), we found a few inclusions (dunites) within three pyroclasts from packet 6.

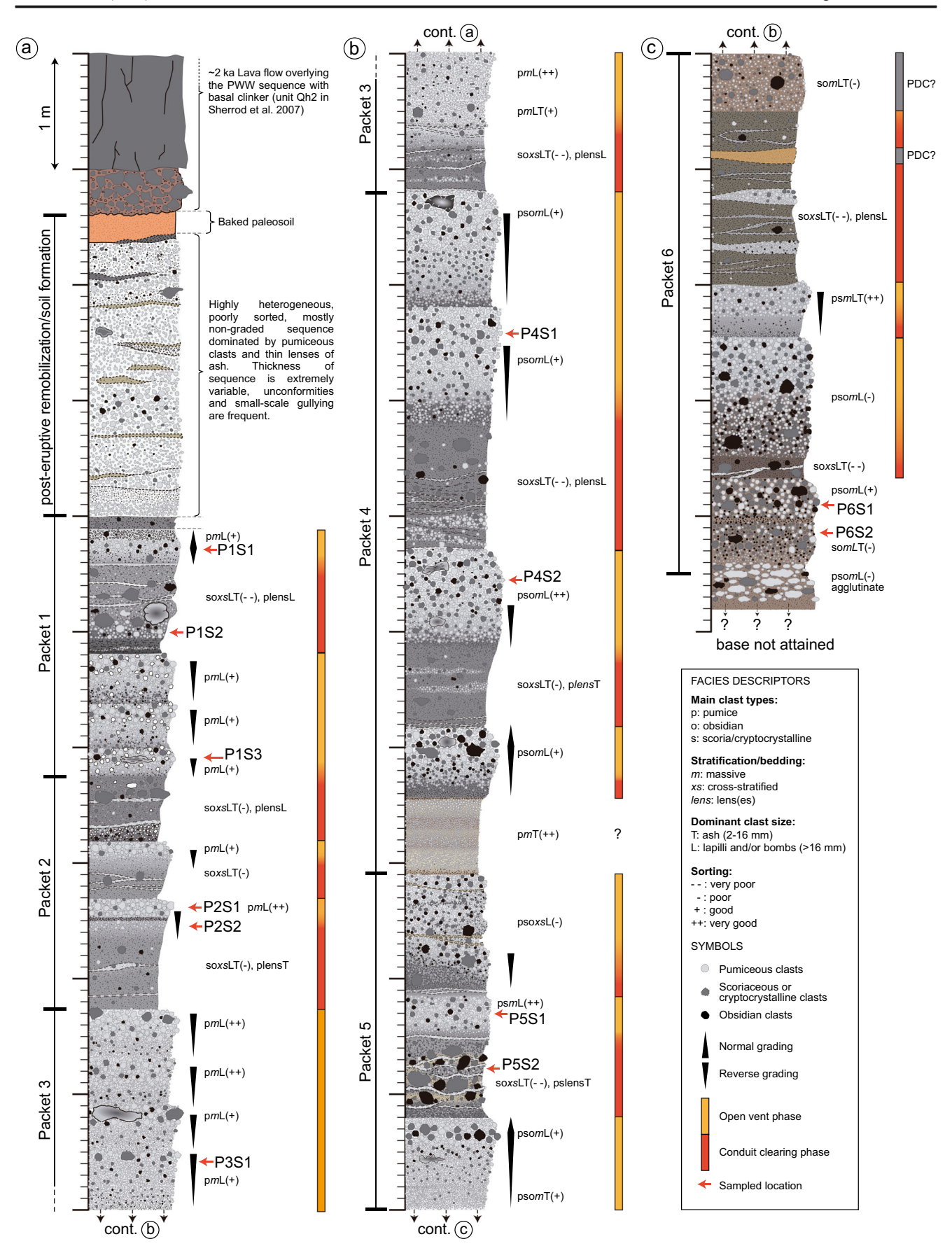
The morphologies and textural attributes of smaller (lapillisized) and larger (block/bomb-sized) pyroclasts are equally variable within the proximal PWW deposits. Large flattened cow dung, ribbon, frothy, or ovoidal bombs occur primarily in the mL facies and often show pumiceous rinds with

scoriaceous to cryptocrystalline interiors (Fig. 5a–i). Obsidian blocks are also common and typically display coarse or fine-scale banding (Fig. 5d). Obsidian and dense microcrystalline blocks are angular and can exhibit breadcrust

Fig. 3 a–c Reconstructed stratigraphy of the Pu'u Wa'awa'a tephra. ▶ Different units were sketched and reported "as is," unless clear evidence of duplexing was recognized (e.g., Fig. 2g), in which case, only one of the duplexed units is shown. Due to this issue of unit repetition and the presence of numerous pinch-and-swell structures, the units were grouped into packets rather than labeled individually



Bull Volcanol (2017) 79:26 Page 7 of 24 26





26 Page 8 of 24 Bull Volcanol (2017) 79:26

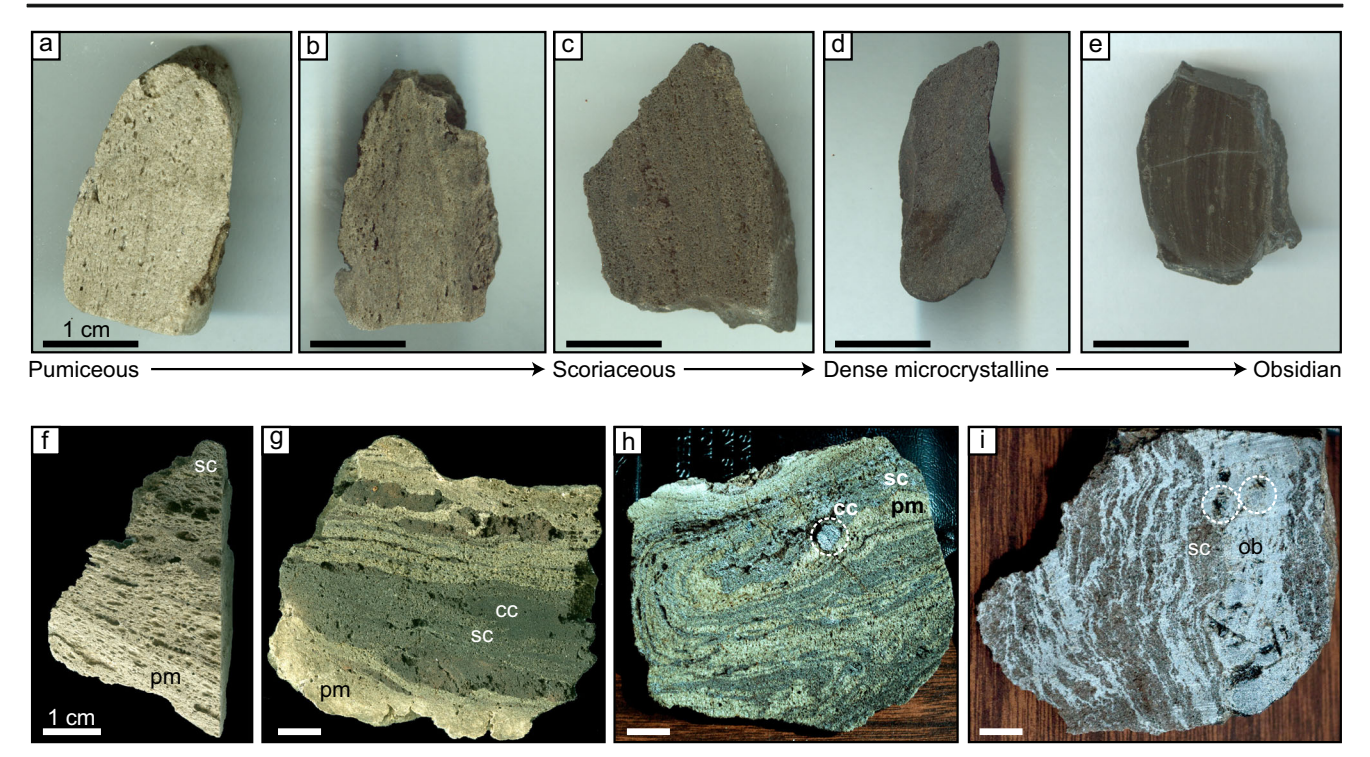


Fig. 4 a–e Diverse pyroclasts collected at Pu'u Wa'awa'a ranked by texture/color type. f–i Textural gradations, banding, and folding within coarse lapilli. pm pumice/pumiceous, sc scoria/scoriaceous, cc cryptocrystalline, ob obsidian/glassy. White dotted circles show cryptocrystalline inclusions

morphologies (Fig. 5g, j) with more vesicular interiors (Fig. 5c-k). Pumice bombs are coarsely vesicular compared to pumice lapilli.

Characteristics of the Pu'u Anahulu flow Only the upper ~10–15 m of the PA can be observed, exposed within gullies that have incised through the superficial portion of the flow. The interior of the flow is not exposed by road cuts, quarrying, or faulting, meaning that our observations are restricted to the upper surfaces. Most of the flow surface consists of dense crypto-to-microcrystalline fractured/brecciated light to dark gray blocks (Fig. 6b–d). The several meters of brecciated carapace are underlain by more competent lava, with a very similar microcrystalline texture to the surface blocks. Banding in the trachyte forms as thin darker gray bands within lighter domains (Fig. 6b) and vice versa (Fig. 6d). The blocky surface is variably altered, blocks being often surrounded by an ochre-colored clay.

**Volume of PA and PWW** Because the medial and distal portions of the PWW tephra are either covered by recent lavas from Hualālai and Mauna Loa or largely eroded, only the cone and the PA flow are considered for volume calculations. The 10-m USGS digital elevation model of Hawai'i was used for cone volume calculations. PA thickness varies substantially (~280 m at its thickest), and we used an average thickness of 120 m integrated across the area inferred for the flow (cf. Fig. 1). These estimates yield minimum volumes of 0.35 km³ for PWW and 3.2 km³ for PA, which are probably conservative

in that both the tephra and lava flow are likely more extensive and thicker under the more recent basaltic flow cover. These volume estimates are lower than the 5.5 km<sup>3</sup> previously inferred by Moore et al. (1987), partly because our inferred PA flow boundaries are more restricted in area.

# Petrology and geochemistry of PWW-PA trachytes

The four main categories of PWW pyroclasts (obsidian, pumiceous, scoriaceous, and cryptocrystalline) and the PA flow samples are compared here with respect to bulk chemistry as well as glass and feldspar compositions to assess whether they share a common origin or, alternatively, derive from different magmas. These data are also compared with that for other trachytes from Hualālai.

Sample mineralogy PWW mineralogy is dominated by feld-spar microlites and microphenocrysts. Subordinate phases include titanomagnetite, apatite, and biotite, all as microlite phases. Large resorbed olivine phenocrysts can be found in glassy obsidian clasts or bands. These olivine grains have high MgO (>Fo<sub>87</sub>, Fo = forsterite content Mg/[Mg + Fe]) and are presumably from disaggregated dunite inclusions picked up during magma ascent (c.f. Clague and Bohrson 1991). Other than the rare xenocrystic phases, no obvious phenocrystic phases (i.e., in the sense of crystals clearly larger than the microlite-microphenocryst population that are cogenetic with the host magma) were found in PWW thin sections.



Bull Volcanol (2017) 79:26 Page 9 of 24 26

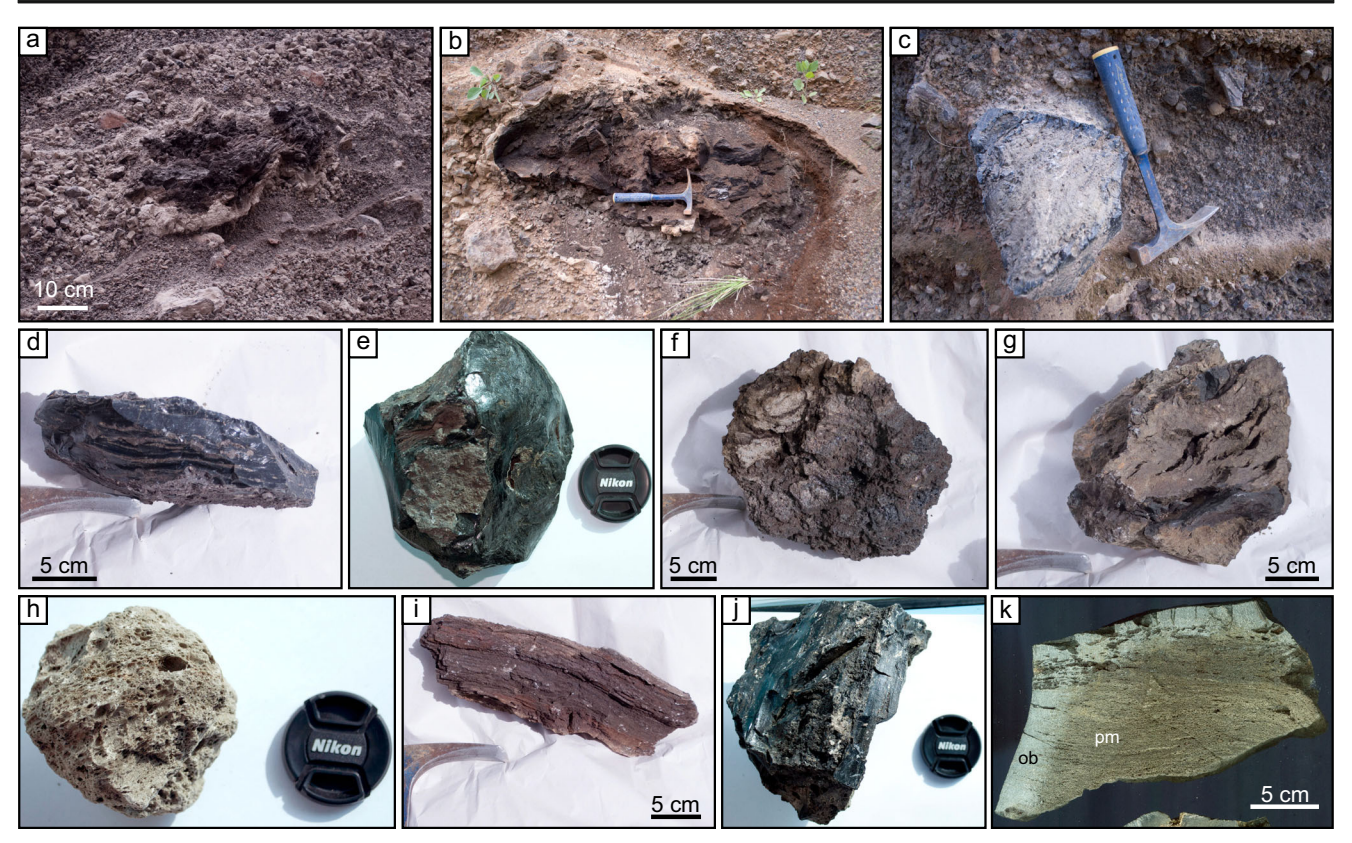


Fig. 5 Variety of blocks and bombs observed in Pu'u Wa awa a tephra. a Cow-dung and b ovoid bombs with thin finely breadcrusted pumiceous rinds and denser scoriaceous interiors. c Angular breadcrusted obsidian block with a more vesicular interior, forming an impact sag on the underyling ash-rich bed. d Platy obsidian block with thin scoriaceous bands. c Dense, angular obsidian block. f-h Frothy and/or breadcrusted

scoriaceous or pumiceous blocks and bombs. **h** Ribbon scoriaceous bomb. **j**, **k** Top and cross section of breadcrusted obsidian block (ob) with pumiceous interior (pm). Note the faint banding in vesicular region and its relationship to obsidian rind suggesting vesiculation continued subsequent to crust formation

PA samples comprise feldspar microphenocrysts ( $\sim$ 150–200 µm along their long dimension), slightly larger on average than their PWW equivalents (typically  $\sim$ 100 µm along their long dimension). Minor phases include dark Fe-Ti oxides, apatite, amphibole, pyroxene, and olivine and rarely exceed 100 µm in length. Small (<20 µm) melt inclusions are sometimes preserved in larger feldspars and Fe-Ti oxides.

Bulk chemistry and glass compositions The lavas making up most of Hualālai's surface are alkali and transitional basalts (+ some Hawaiite). Subaerial tholeiites are less common but have been recovered in submarine dives and dredges (Clague et al. 1980; Moore et al. 1987; Moore and Clague 1992; Lipman and Coombs 2006; Hammer et al. 2006; Hanano et al. 2010) (Fig. 7a). A large compositional gap exists between the alkalic basalts and the trachytes of Hualālai. Diorite xenoliths enclosed in recent basaltic eruptions are the only known potential intermediate magma between the basalts and trachytes (Shamberger and Hammer 2006). As previously noted by Cousens et al. (2003), PWW and PA bulk compositions differ in major and minor elements, with PWW samples higher in MnO, K<sub>2</sub>O, and Na<sub>2</sub>O but lower in Al<sub>2</sub>O<sub>3</sub>, TiO<sub>2</sub>, and

MgO (Fig. 7b–d). These compositions also differ from the Waha Pele (WP) and Huehue (HH) trachyte blocks (Clague and Bohrson 1991; Cousens et al. 2003), which are more SiO<sub>2</sub>, TiO<sub>2</sub>, and MgO rich, and FeO and Na<sub>2</sub>O poor than PWW and PA. The four different trachyte compositions (PWW, PA, WP, and HH) do not lie on any clear binary mixing or differentiation trend.

Glasses from PWW cover a broad range in composition, generally tracking the feldspar crystallization control line (Fig. 7b–d). The PWW glass compositions are also distinct from those of the Hualālai ignimbrites (HI) that overlie the PA flow, which prompted Shea and Owen (2016) to assume different origins for these two units.

Mineral compositions Feldspar microlites and microphenocrysts in the PWW and PA samples are anorthoclase (cf. Supplementary Material Fig. A1). Microlites are usually fairly homogeneous in composition, while microphenocrysts can display sector or boxwork zoning patterns. Although feldspar compositions partly overlap, PWW anorthoclase is typically more Ab rich while PA anorthoclase is slightly more Or rich.



26 Page 10 of 24 Bull Volcanol (2017) 79:26

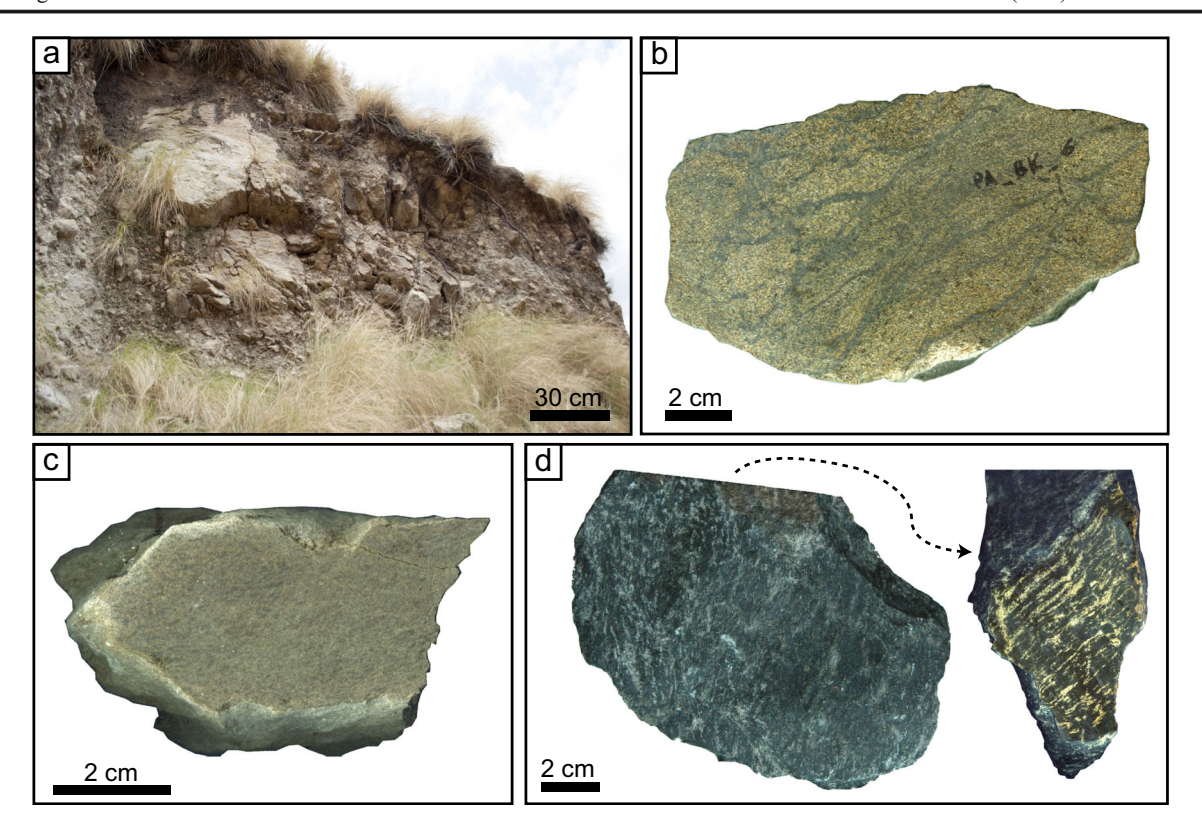


Fig. 6 a Blocky brecciated upper zone of the Pu'u Anahulu flow. b Banded trachyte block. Thin dark bands consist of a finer grained anorthoclase cryptocrystalline matrix whereas other regions are

microcrystalline and show diktytaxitic textures.  ${\bf c}$  Light homogeneous microcrystalline trachyte.  ${\bf d}$  Dark banded trachyte similar to  ${\bf b}$  but with dark regions dominant

Oxides in PWW and PA are almost exclusively titanomagnetite (with  $\sim 15$  wt% TiO<sub>2</sub>), and a thorough search for coexisting ilmenite failed to identify any grains that were suitable for thermo-oxybarometry. Olivine in the PA samples is MnO rich (i.e.,  $\sim 5$  wt%), and fayalitic (Fo<sub>40</sub>). Amphibole compositions correspond to Fe-rich edenite, and pyroxenes are aegirine-augite.

Because the minerals are usually small and, except for larger feldspars, unzoned, it is unclear whether any of the phases present in these rocks could have formed during storage at depth. Instead, we interpret the vast majority of crystals present in the PWW and PA samples to have formed at shallow levels during magma ascent, and, in the case of PA, during lava flow emplacement. Considering that rapidly grown microlites or microphenocrysts are likely to show disequilibrium compositions (e.g., Martel and Schmidt 2003; Brugger and Hammer 2010), we did not apply thermo-barometers to these units.

# Textural characteristics of pyroclasts

Componentry The four main classes of pyroclasts identified (pumiceous, scoriaceous, cryptocrystalline, and obsidian) are present within all the units sampled from the six packets. Within packets 1–4 and the top unit of packet 5, pumiceous clasts are most abundant (≥50% of the total number of clasts), usually followed by cryptocrystalline clasts and similar

amounts of scoriaceous and obsidian end-members (Fig. 8a). The bottom three units of the sequence (bottom of packet 5, packet 6) contain less pumice (<50%) and comparatively more cryptocrystalline, obsidian, and scoriaceous clasts than the overlying units. Breccia clasts are found only occasionally. From bottom to top of the sampled stratigraphy, there appears to be a crude decrease in the abundance of dense clasts and increase in pumiceous clasts (Fig. 8a).

**Vesicularity and vesicle textures** Vesicularities range from 0 to 85% in the PWW pyroclasts. The density distributions are broadly bimodal (with the exception of unit 551), with modes at  $\rho = 0.6$ –0.7 g cm<sup>-3</sup> and  $\rho = 1.7$ –2.2 g cm<sup>-3</sup> (Fig. 8b). The visual classification of pyroclasts into four textural categories corresponds well with vesicularity/density groupings, with pumiceous clasts showing high vesicularity (40–85% vol., Figs. 8b and 9a, d), obsidian, and cryptocrystalline clasts belonging to the low vesicularity end of the spectrum (<30% vol., Figs. 8b and 9b–i) and scoriaceous clasts having a wide range of vesicularities (20–70% vol., Figs. 8b and 9g–h).

Vesicles in pumiceous clasts display a wide range of shapes (equant to elongated), generally have smooth outlines, and are frequently coalesced (Fig. 9a, d). In contrast, vesicles in scoriaceous clasts and low vesicularity obsidian have irregular shapes and outlines (Fig. 9b–h), while those preserved in cryptocrystalline and obsidian



Bull Volcanol (2017) 79:26 Page 11 of 24 26

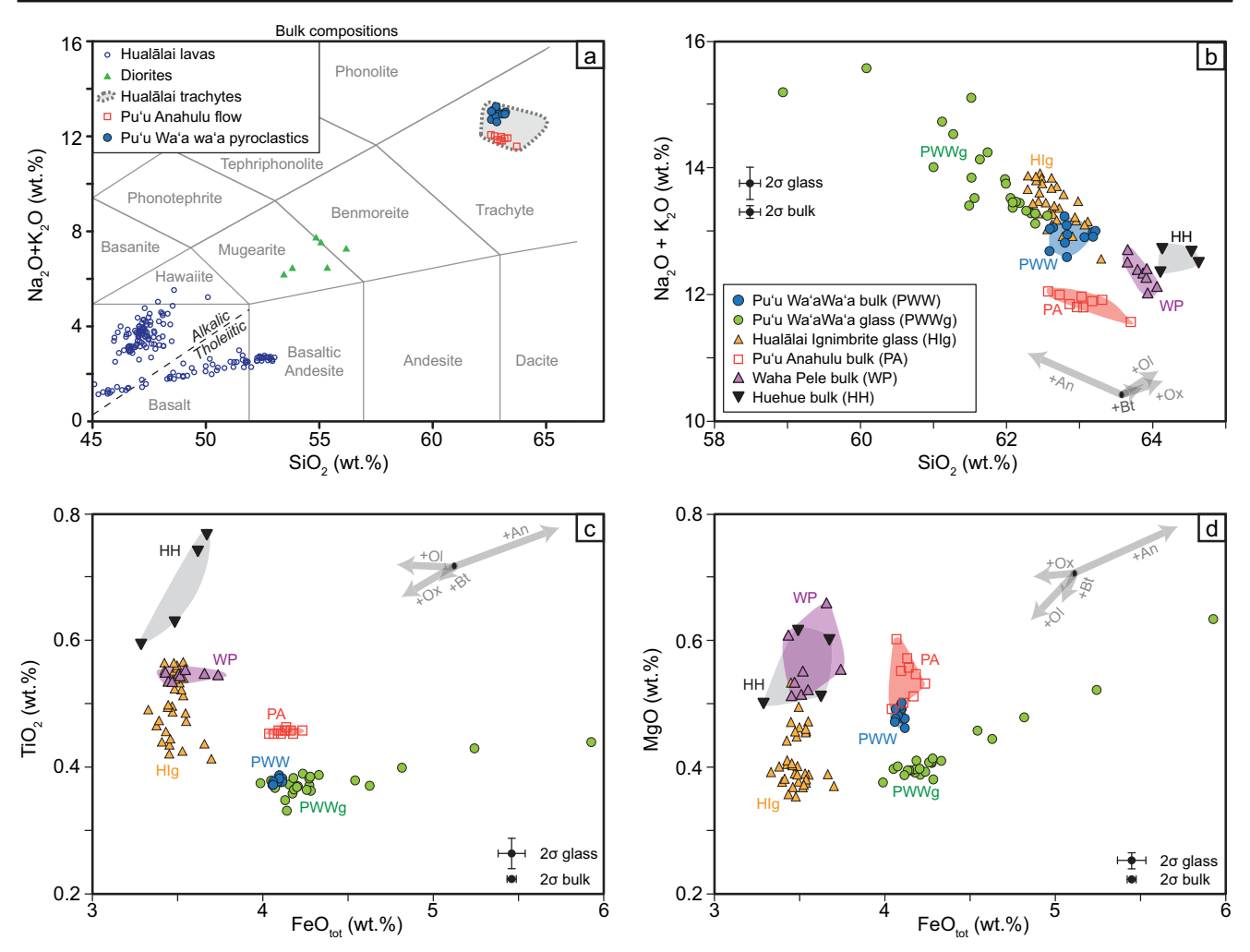


Fig. 7 Major element composition of Hualālai trachytes (modified after Shea and Owen 2016). a Bulk composition of Hualālai volcanics illustrating the important gap from typical shield-stage and post-shield stage basalts (tholeiites and alkali basalts) to trachytes (data from Macdonald 1968; Clague et al. 1980; Moore et al. 1987, Moore and Clague 1992; Hammer et al. 2006; Lipman and Coombs 2006; Hanano et al. 2010).

Diorite xenoliths included within recent basalt may represent the only known intermediate lithologies (Shamberger and Hammer 2006). **b**–**d** Glass and bulk composition plots for the different trachytes collected at Hualālai. *Arrows* show crystallization path involving the principal phases found in the trachytes (amphibole and pyroxene are rare and were omitted). Average precision is reported for both glass and bulk analyses

clasts are very small (generally <10  $\mu$ m) and equant (Fig. 9c–i). Vesicularities and vesicle shapes can be highly variable at the clast scale, which, in combination with heterogeneous distribution of microlites, produce macroscopic banding of the pyroclasts (cf. Supplementary Material Fig. A2). Heterogeneity in pumiceous clasts also takes the form of localized shear zones.

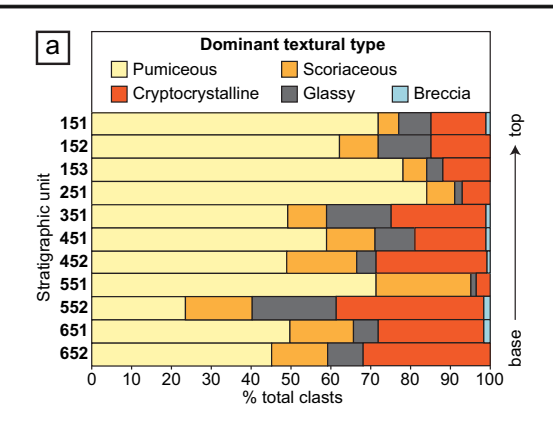
Crystallinity and feldspar textures Feldspar abundances vary widely between different PWW samples. Obsidian and pumiceous samples contain the fewest microlites/microphenocrysts (0–15% vol. with an average of 6.5% vol., Fig. 9a–d), followed by scoriaceous (~10–40% vol. with an average of 21% vol., Fig. 9e–h) and cryptocrystalline clasts (25–50% vol. with an average of 36% vol., Fig. 9f, i). Feldspars are generally tabular, with maximum lengths

≤250 µm and widths ≤20 µm. In high-crystallinity samples or high-crystallinity regions of heterogeneous clasts, webs of thin filamentous feldspars connect the larger microphenocrysts (Fig. 9i). Heterogeneity in PWW samples is often expressed as microlite enrichment zones, with a variably intense bandparallel alignment of feldspars (Fig. A2). In samples or bands that lack a clear fabric, crystals are often arranged as microspherulites or axiolites. Banding is also produced by variably deformed inclusions, blebs, or even entire zones of microcrystalline trachyte. Breccia clasts consist of agglomerated particles of various sizes that display the entire spectrum of crystallinities observed in the four different textural categories.

PA samples are holocrystalline, consisting mostly of feld-spar and small oxides as interstitial phases. Samples display a classical "trachytic" texture (Fig. 9j–l), with generally parallel, imbricated tabular anorthoclase crystals ≤700 µm in length.



26 Page 12 of 24 Bull Volcanol (2017) 79:26



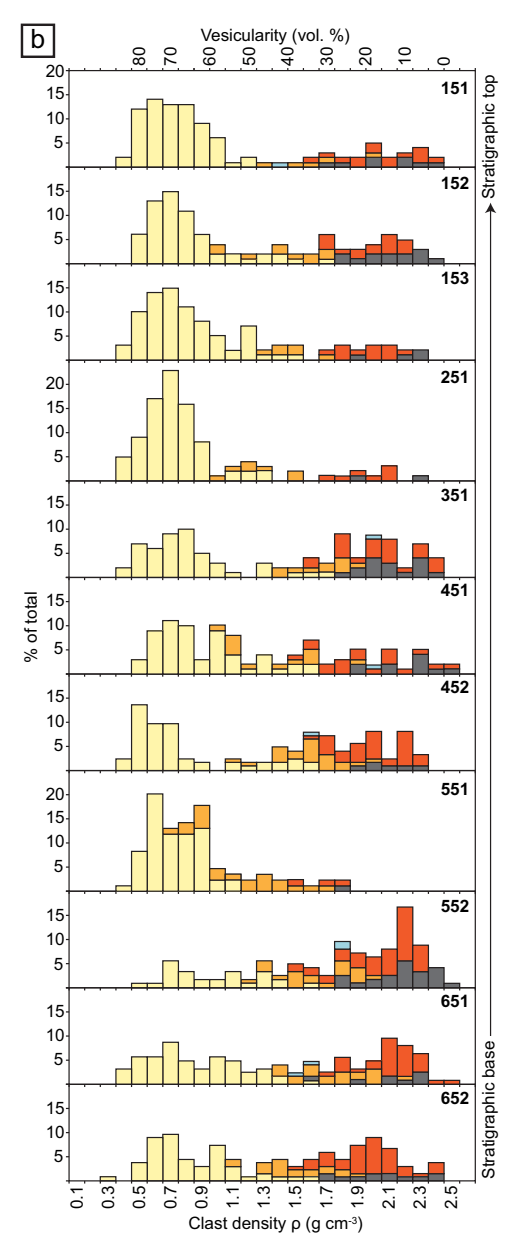
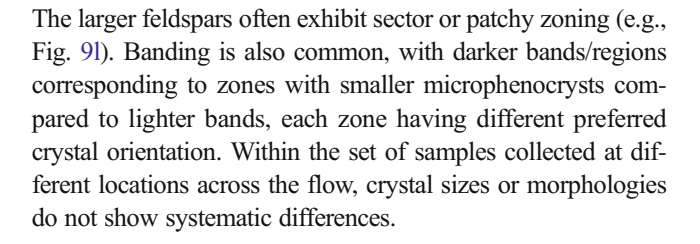


**Fig. 8** a Componentry (by texture type) of Pu'u Wa awa a pyroclasts from different units sampled. **b** Clast density/vesicularity distributions for the same units. Overall, the range in density is large and distributions are typically bimodal



# Relationship between vesicularity and crystallinity

Samples analyzed for feldspar abundance show at least two different behaviors with respect to vesicularity (Fig. 10a). One set of clasts follows a high vesicularity path, where crystallinity increases as vesicularity decreases from 83 to 40%. A second set of clasts defines a low vesicularity path, where a steep decrease in vesicularity with increasing crystallinity is followed by a path of nearly constant low vesicularity (~0–10% vol.).

Vesicularity alone is not a good measure of magma degassing/outgassing processes because low values can correspond either to the initial vesiculation stage or final stages of gas escape and bubble collapse (e.g., Shea et al. 2012; Giachetti and Gonnermann 2013). The extent of microlitemicrophenocryst crystallization is a more robust indicator of how long a magma has spent near the surface after decompression-induced devolatilization (e.g., Hammer et al. 1999). With this in mind, the two decreasing crystallinity vs. vesicularity trends (Fig. 10a) mostly track the outgassing process (bubble interconnection and collapse). The low vesicularity path potentially records a "rapid" outgassing path where permeability development and foam collapse are rapid (i.e., vesicularities reach 0-10% after <10% vol. feldspar crystallization), whereas the high vesicularity path records a history marked by slower outgassing (termed "slow" outgassing, Fig. 10a). Both outgassing paths are ultimately effective in that both obsidian and cryptocrystalline clasts attain near zero vesicularities, but microlite content clearly distinguishes them in terms of outgassing paths and probably rates. The major element chemistry of interstitial glass in PWW samples is also consistent with this degassing-induced crystallization history. Low crystallinity samples (pumiceous and obsidian) show low to moderate K<sub>2</sub>O enrichments, while highly crystalline samples (scoriaceous and cryptocrystalline) occupy the high K<sub>2</sub>O end of the spectrum (Fig. 10b).

# Volatile contents

No  $\mathrm{CO}_2$  was detected by FTIR (only obsidian clasts analyzed) or Raman (all types of clasts). Glass  $\mathrm{H}_2\mathrm{O}$  measured by microRaman varies between 0.15 and 2.1 wt% (Fig. 10c). High concentrations (>1 wt%) are only measured in scoriaceous and pumiceous samples, which also display the largest variability. Obsidian clasts typically have less than 0.5 wt%  $\mathrm{H}_2\mathrm{O}_{tot}$  and cryptocrystalline samples around 0.5–1.0 wt%. A transect performed across a banded obsidian-cryptocrystalline clast confirms



Bull Volcanol (2017) 79:26 Page 13 of 24 26

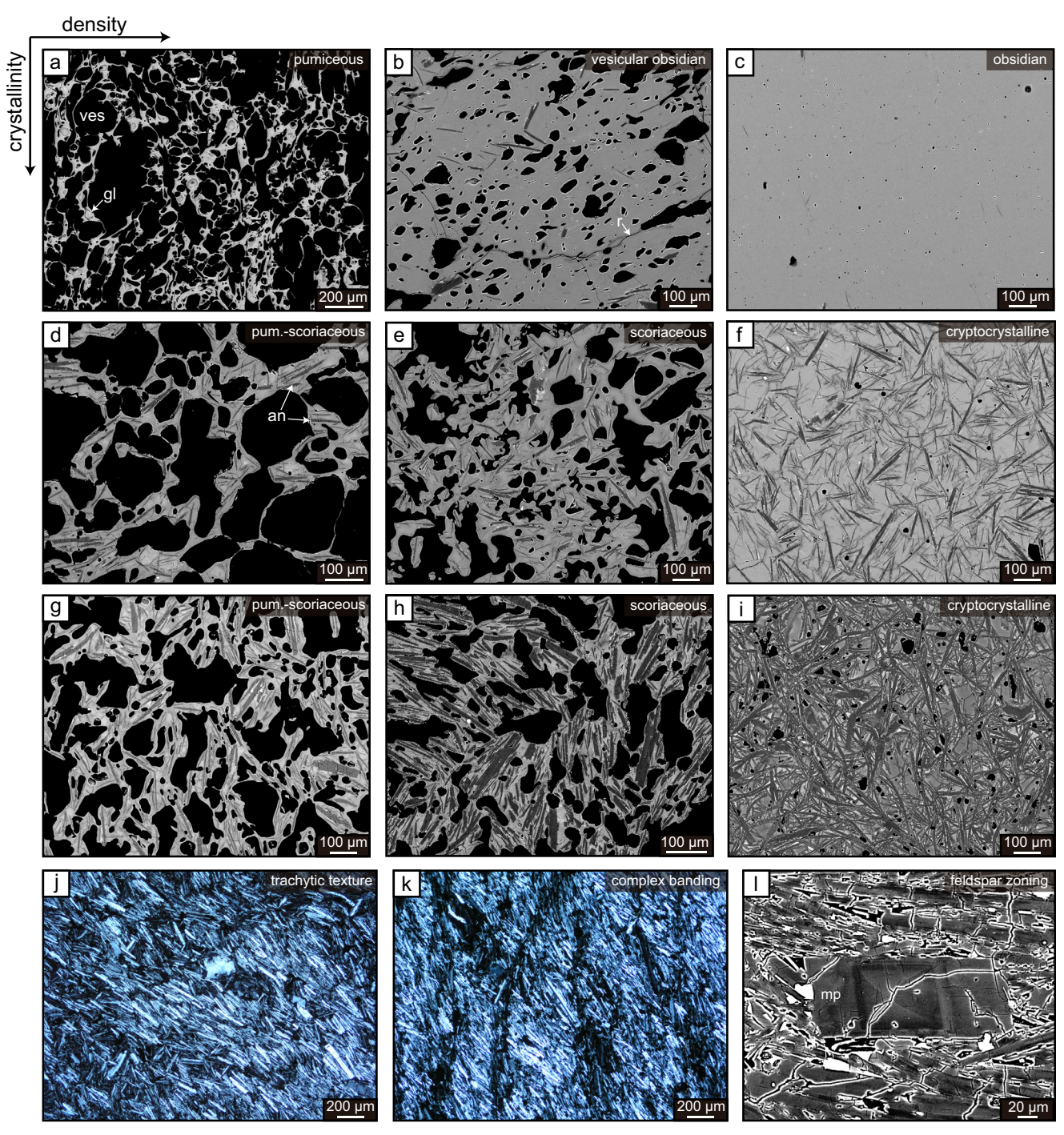


Fig. 9 Backscatter electron images and microphotographs from Pu'u Wa awa a (a-i, rows sorted by decreasing vesicularity, columns by increasing crystallinity) and Pu'u Anahulu (j-l) trachytes. The fairly homogeneous grayscale in most PWW microlites and microphenocrysts

indicates little compositional variation in the major elements, while larger microphenocrysts (mp) in PA lavas regularly display complex zoning patterns

that cryptocrystalline textures correspond to slightly higher  $H_2O_{tot}$  values (Fig. 10d). Transects and maps acquired at the edge of an obsidian sample, combined with TGA measurements, clearly demonstrate that rehydration has affected all pyroclast glasses and, in the worst cases, increasing measured  $H_2O$  to >2 wt% (see Supplementary Material and Figs. A3 and A4).

The high  $H_2O$  in cryptocrystalline glasses relative to obsidian samples (Fig. 10c, d) cannot be easily explained by processes of secondary hydration, however. The low vesicularity (<15%), the large separation between vesicles, and the presence of microlites near glass where  $H_2O$  was measured together preclude significant incorporation of meteoric water in the glass by



26 Page 14 of 24 Bull Volcanol (2017) 79:26

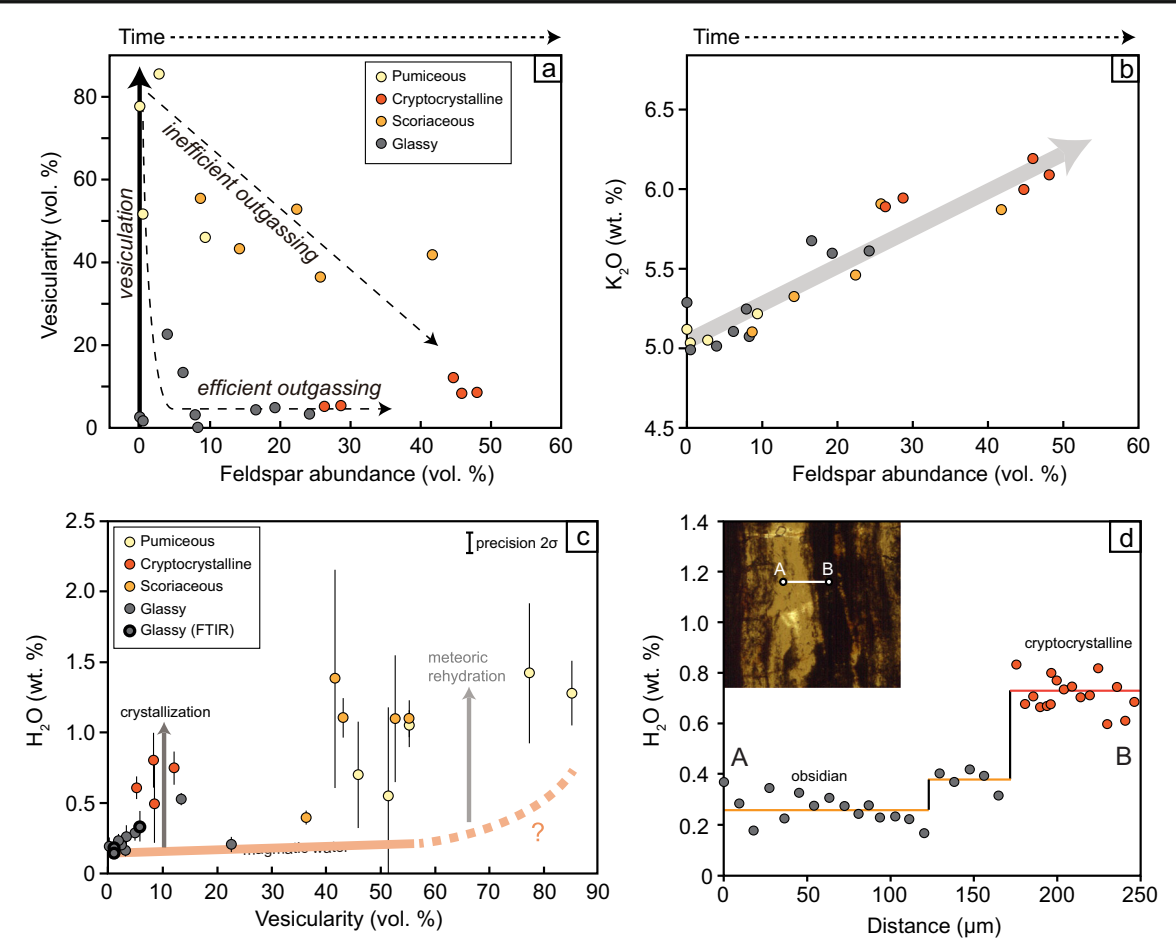
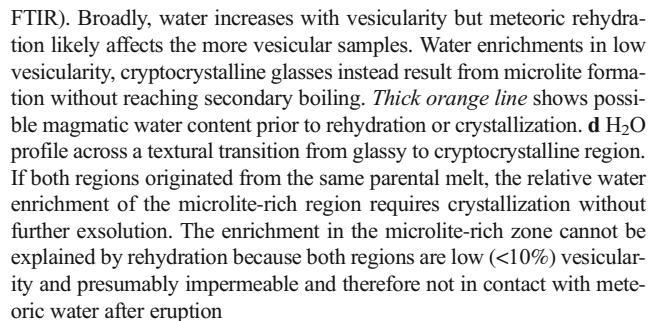


Fig. 10 Indicators of crystallization and degassing/outgassing in Pu'u Wa'a wa'a pyroclasts. a Pyroclast vesicularity vs. feldspar abundance for different textural types. Microlite crystallization is strictly a function of time during/after degassing, and two possible outgassing paths are shown. During "rapid" outgassing, pumiceous clasts quickly become gas poor and crystallize variably as a function of residence time at high temperature in the conduit. During "slow" outgassing, the pace of crystallization roughly keeps up with permeable gas loss. b Glass  $K_2O$  content as a function of feldspar abundance, confirming that all samples originate from a similar initial melt, the matrix glass composition being merely a function of microlite content. c Glass H2O measured by Raman for different clast types (three glassy samples were also measured by

diffusion. Instead, we propose that the relatively high  $\rm H_2O_{tot}$  contents in highly crystalline samples result from microlite crystallization and enrichment of the residual melt in water without reaching the point of exsolution and secondary boiling.

# **Discussion**

Our results shed light on the volcanological history of the enigmatic Hualalai trachytes and provide the basis for several major discussion points. We first show that contrary to previous interpretations, PWW and PA were not produced during the same eruption. We then examine the eruption dynamics at PWW, incorporating the evidence provided by deposit



architecture and by the textural information supplied by extremely varied pyroclast populations. We develop a transitional violent-Strombolian-Vulcanian eruption model that is consistent with the various observations. We then consider the implications of these new findings for the diversity of trachyte eruption styles in Hawai i and examine some key differences between trachytes and other evolved magmas.

# Are Pu'u Wa'awa'a and Pu'u Anahulu related to the same eruption?

The Pu'u Wa'awa'a tephra sequence and the Pu'u Anahulu flow were never found in stratigraphic contact. Bulk and interstitial glass compositions from Pu'u Wa'awa'a pyroclasts



Bull Volcanol (2017) 79:26 Page 15 of 24 26

differ from the composition of the Pu'u Anahulu flow. Clasts with PA mineral textures or compositions were not found as wallrock in the cone deposits, intimating that the PA flows had not yet been erupted when the PWW cone formed. This hypothesis is also supported by the lack of PWW deposits on top of PA or the Hualālai ignimbrites that postdate PA (Shea and Owen 2016). The small compositional difference between PWW and PA could indicate a zoned trachyte reservoir. However, the bulk compositions of PWW and PA do not align along obvious fractional crystallization trends (i.e., they cannot be obtained by crystallization of a single parental magma), meaning that compositional zoning in the reservoir would have to result from injection of a different trachyte (Fig. 7). We favor instead the idea that PWW and PA tapped independent reservoirs and were erupted separately in time and space. More generally, the lack of clear association between PA and PWW magmas supports the hypothesis that at least four Hualālai trachytes (PWW, PA, the Hualālai ignimbrites, and the Huehue trachytes) were erupted from compositionally distinct reservoirs (Shea and Owen 2016).

# Pyroclastic density currents or syn-eruptive remobilization of proximal fall deposits?

Pinch-and-swell stratification is common in both PDC deposits and proximal fallout facies that undergo downslope remobilization (Branney and Kokelaar 2002). Distinguishing between the two is not straightforward as both processes involve lateral movement of tephra, making deposit interpretations more challenging in near vent regions. Within the PWW sequence, the presence of pinch-and-swell structures, lenses, and the poor sorting seen in many subunits can therefore be read as evidence for either pyroclastic density currents or remobilization of fall layers. Similar lithofacies and reverse grading can be found in scoria cones and have been termed grainflow or granular flow deposits (Branney and Kokelaar 2002; Valentine et al. 2005; Alvarado et al. 2011; Cagnoli et al. 2015). We interpret most of the PWW units to also reflect syn-eruptive remobilization and fall deposits on a near repose-angle slope. It is unlikely that rapidly moving PDCs would preserve pumice angularity within the wellsorted lapilli units or the integrity of breadcrust or cowdung bombs (Fig. 5a, b). The presence of impact sags under large dense bombs (e.g., Fig. 5c) suggests that some large clasts fell as beds were remobilized downslope. Blocks and bombs within the cross-stratified base of PWW fall units, interpreted as ballistic clasts, may have also enhanced remobilization and grainflow following their impact. Although large-scale PDC deposits were not found within the PWW quarry, two to three poorly sorted, slightly indurated ash-rich layers in packet 6 may have formed from small, fairly dilute PDCs (Figs. 2g and 3).

# Origin of textural variability of Pu'u Wa wa a pyroclasts

The striking textural diversity of PWW pyroclasts with respect to color, vesicularity, microlite content, and banding (Fig. 4) has several possible origins: (1) mixing/mingling of different magmas (e.g., Sigurdsson et al. 1990; Klug and Cashman 1994; Polacci et al. 2001; Rosi et al. 2004; Wright et al. 2011), (2) highly variable magma degassing paths in space and time within the conduit (e.g., Hammer et al. 1999; Lautze and Houghton 2007; Neill et al. 2010; Giachetti et al. 2010; Shea et al. 2012), and/or (3) recycled material from prior explosions forming additional rheological layers at the top of the conduit as underlying magmas reheat the deposited pyroclast pile (e.g., Gurioli et al. 2014; Leduc et al. 2015). Bulk compositions of PWW pyroclasts are similar for different textural end-members (Fig. 7 and Table A1, Shea and Owen 2016). Glass compositions are largely controlled by feldspar crystallization (Figs. 7b-d and 10b). Both observations argue against significant magma mixing or compositional changes during magma ascent. While some amount of material was probably recycled from each explosion and possibly reheated by underlying magma, this material would not produce glassy, microlite-poor obsidian clasts or pumice. Therefore, we suggest that this textural diversity was mostly related to magma degassing/outgassing processes likely occurring in the conduit.

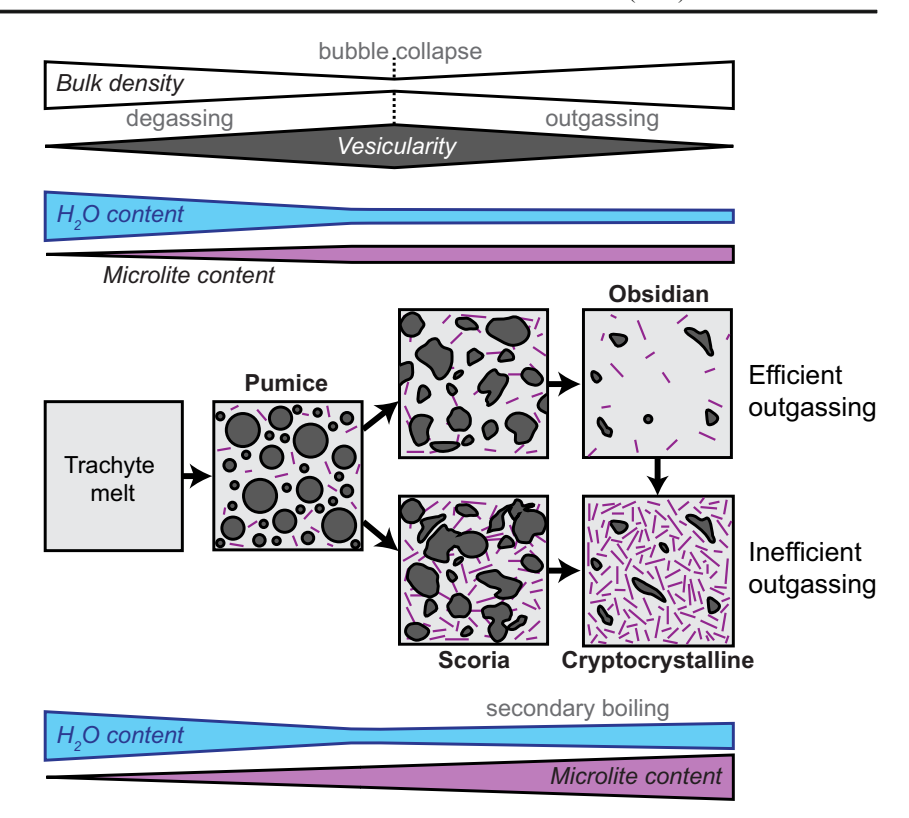
In the absence of measured  $CO_2$ , we infer that vesiculation and microlite crystallization were controlled by loss of magmatic  $H_2O$  from the melt (e.g., Geschwind and Rutherford 1995; Hammer et al. 1999; Clarke et al. 2007). The remarkable variety of pyroclast textures can be reconciled by variable decompression paths (Fig. 11):

- 1. Pumiceous clasts represent the earliest stage of degassing recorded in our pyroclast collection.
- 2. Obsidian clasts, with very low H<sub>2</sub>O contents and crystal-linities (Fig. 10a), are inferred to derive from permeable outgassing (bubble coalescence and collapse) of initially vesicular, microlite-poor magma. For the glassy textures to be preserved, obsidian clasts must have cooled rapidly and/or had short residence times in the conduit after bubble collapse.
- 3. Scoriaceous experienced protracted degassing and outgassing, allowing for substantial crystallization (Fig. 10a). The coarse irregular vesicles in scoriaceous clasts and their moderate to high crystallinity suggest they preserve a record of slower outgassing compared to magmas that formed the obsidian.
- 4. Cryptocrystalline clasts resided the longest at high temperatures in the conduit and may have formed by crystallization of the same crystal-poor magma that generated obsidian or by further outgassing and crystallization of scoriaceous clasts. Those two paths towards formation of



26 Page 16 of 24 Bull Volcanol (2017) 79:26

Fig. 11 Interpretive sketch of how pyroclast textures (density, vesicularity, and microlite contents) may relate to H2O degassing and outgassing. All samples had the same starting melt. Pumice clasts represent here the earliest records of the degassing process, and all samples with lower vesicularities preserve the subsequent outgassing history. The upper row shows a "rapid" outgassing path (see Fig. 10a) where bubble coalescence, collapse, and permeable outgassing occur rapidly, before microlites can crystallize to a significant extent (ultimately resulting in crystal-free or crystalpoor obsidian). Bottom row shows the "slow" outgassing path where crystallization and outgassing occur at the same time (resulting in scoriaceous clasts). Both paths can lead to cryptocrystalline textures with sufficient time



- cryptocrystalline clasts are here termed "rapid" and "slow" outgassing paths (Fig. 10a). During rapid outgassing, gas loss precedes most crystallization whereas during slow outgassing, gas loss and microlite formation are coeval.
- 5. The color of different pyroclast types is controlled by vesicle and feldspar contents, Fe-Ti oxides, and Fe<sup>3+</sup> vs. Fe<sup>2+</sup> in the glass (e.g., Paulick and Franz 1997). Raman spectra clearly show an increase in the Fe<sup>3+</sup> content of the glass from the microlite-free and pumiceous clasts (low relative Fe<sup>3+</sup>/Fe<sup>2+</sup>) to the scoriaceous and cryptocrystal-line clasts (high relative Fe<sup>3+</sup>/Fe<sup>2+</sup>) (Di Muro et al. 2009, Di Genova et al. 2016; cf. Fig. A5 in the supplementary material). The higher Fe<sup>3+</sup> content in microcrystalline and scoriaceous clasts also suggests that they either derived from regions of slower cooling rates in the shallow upper conduit under oxidizing conditions. Dense clasts may have oxidized further after emplacement in the cone as the deposits slowly cooled.

Although few small-volume trachyte eruptions have been analyzed for pyroclast characteristics, tephra from the trachyphonolitic AD1538 Monte Nuovo eruption (Campi Flegrei, Italy) displays a similar range in textures (D'Oriano et al. 2005; Polacci et al. 2014). There, clasts also include small pieces of obsidian, microlite-rich scoria, and pumice that are all indistinguishable in composition and were interpreted to reflect variable lateral extents of degassing and residence times in the

conduit. Diverse pyroclast textures, including the presence of variably microlite-rich pyroclastic obsidian and darker and lighter pumice, have also been observed in rhyolitic pumice cones (e.g., Monte Pilato, Davì et al. 2011), although such tephra seems to lack microlite-rich scoriaceous and cryptocrystalline end-members. At the other end of the compositional spectrum, pyroclasts from basaltic or basaltic-andesitic cinder cones (e.g., Croscat, Cimarelli et al. 2010; Paricutin, Pioli et al. 2008) share scoriaceous and dense cryptocrystalline textures but rarely contain substantial amounts of microvesicular pumice and lack glassy obsidian. Pu'u Wa'awa'a is therefore unusual in encompassing pyroclast characteristics from the entire compositional range of cone-building eruptions.

# Eruption dynamics at Pu'u Wa'awa'a

Inferring an eruption style is a challenge without a clear picture of how the PWW tephra is distributed or how grain size varies away from the cone. Our inferences about eruption dynamics are therefore based exclusively on proximal deposit architecture and pyroclast characteristics. An adequate eruption model for PWW needs to account for (1) the textural diversity of pyroclasts and their inferred degassing/outgassing history (Figs. 8, 10, and 11), (2) the repeated pattern of cross-stratified, dense-juvenile-rich lithofacies overlain by well-sorted pumice lapilli beds (Fig. 3), (3) the presence of breadcrust and other types of bombs within the cross-stratified subunits (Fig. 5), and (4)



Bull Volcanol (2017) 79:26 Page 17 of 24 26

the absence of basaltic wallrock or other lithic components. In this section, each key observation is discussed in the context of potential eruption dynamics.

The broad, often bimodal pyroclast density/vesicularity distributions throughout the exposed PWW sequence are similar to deposits of Vulcanian eruptions involving domes or cryptodomes (Kilian 9400 BP; Chachimbiro 3640-3510 BC; phase 4 of Novarupta 1912 AD; Bezymianny 1956 CE; Mt. St Helens 1980 CE; Hoblitt and Harmon 1993; Adams et al. 2006; Belousov et al. 2007; Neill et al. 2010; Bernard et al. 2014; Colombier et al. 2017), or conduit plugs (Soufrière Hills 1997 CE; Formenti and Druitt 2003; Giachetti et al. 2010). These deposits also revealed large variabilities in vesicularity and microlite crystallinity, with dense material linked to an outgassed, more microlite-rich dome or plug and vesicular microlite-poor material with underlying volatile-rich magma (e.g., Clarke et al. 2007; Neill et al. 2010; Giachetti et al. 2010). The abundance of dense juvenile clasts and their textural and volatile characteristics suggest a similar conduit configuration for Pu'u Wa'awa'a with the added requirement of having both outgassed microlite-free (obsidian) and microliterich (cryptocrystalline) magma erupted simultaneously.

The repeated transition in the PWW deposits from poorly-sorted units rich in dense clasts to well-sorted pumice-rich units is also consistent with an eruption style that involves clearing of a dense, partly solidified magma column followed by ejection of frothy magma. Breadcrust obsidian and cryptocrystalline blocks found within the cross-stratified facies are also similar to ballistics found in Vulcanian deposits (Wright et al. 2007; Giachetti et al. 2010). The residual water contents of obsidian clasts from PWW ( $H_2O_t \sim 0.15-0.20$  wt%) correspond to very low equilibrium solubility pressures of <5 MPa (Di Matteo et al. 2004) and quenching depths <150 m, assuming a lithostatic pressure gradient. In addition, while microlites often display preferential alignment within PWW obsidian, the lack of alignment or elongation of vesicles indicates sufficient time for bubbles to relax following ascentrelated shearing/stretching. Similar non-dynamic conditions are also required to explain the microspherulite textures observed within some of the obsidian clasts.

Unlike most Vulcanian eruptions studied to date, however, deposits of the PWW eruption show no clear evidence for large pyroclastic density currents. PDCs produced during Vulcanian eruptions can be generated by collapse of extruded domes or cryptodome explosions (e.g., Hoblitt and Harmon 1993; Belousov et al. 2007) and can also accompany fallout plumes during explosions involving plugs that are restricted to the conduit (e.g., the Soufrière Hills explosions of August and September 1997; Druitt et al. 2002). More importantly, Vulcanian eruptions rarely construct tephra cones, which are more typical of violent Strombolian or Hawaiian eruptions (e.g., Valentine et al. 2005; de Silva and Lindsay 2015).

The PWW eruption did not involve significant interactions with non-magmatic water. The only non-juvenile materials found within the entire PWW sequence are a few <1-cm dunite inclusions (see also Clague and Bohrson 1991) and basaltic wallrock—likely ubiquitous around and underneath the PWW vent—or foreign trachyte is lacking. Therefore, we infer that the cone was formed during a purely magmatic eruption, although we cannot discard the possibility of earlier phreatomagmatism, common during opening phases (e.g., Laacher See, Schmincke et al. 1999; Monte Nuovo, D'Oriano et al. 2005).

In light of the key observations addressed above, we envision that the Pu'u Wa'awa'a tephra was produced by a dominantly magmatic eruption, transitional in style between violent Strombolian (i.e., prolonged through several months or more, with high enough overall eruption rates to build large cones, pulsatory, e.g., Valentine et al. 2005; Pioli et al. 2008; Andronico et al. 2009; Di Traglia et al. 2009) and Vulcanian (i.e., transient, including formation and disruption of a conduit obstruction; e.g., Druitt et al. 2002; Clarke et al. 2015). Each eruption cycle at PWW began with overpressurization and disruption of a conduit plug that was at least partly solidified (Fig. 12). Material from the plug was first evacuated and produced the lithofacies at the base of the sequence rich in obsidian and cryptocrystalline clasts. Vesicular magma shortly followed to generate pumice-lapilli-rich fall units. Ascent rates progressively decreased in concert with conduit overpressure. The top of the magma column became largely permeable and outgassed quiescently (e.g., Eichelberger et al. 1986) potentially through localized shear zones and/or fractures (e.g., Edmonds et al. 2003; Cabrera et al. 2011; Schipper et al. 2013; Lavallée et al. 2013). The top of the column (and possibly fallback material) solidified into an obsidian-rich outgassed carapace. The interior of the plug cooled more slowly and crystallized, later producing the cryptocrystalline clasts. Deeper magma with more residual gas outgassed less rapidly and produced magma that fragmented to scoriaceous clasts during the next overpressurization sequence. The lack of significant PDC deposits indicates that no significant dome was constructed between explosive cycles and that the eruption column did not experience significant destabilization. Compared to other tephra cones constructed during mono- or polygenic violent Strombolian activity (e.g., Paricutin, Mexico; Cerro Negro, Nicaragua), the Pu'u Wa'awa'a edifice is significantly larger (cf. Fig. A6 in the Supplementary Material), consistent with a slightly higher intensity and/or a longer eruption. Comparisons of PWW deposit characteristics (deposition modes, pyroclast types, and textures) with other trachyte cones are difficult because the only example thoroughly examined involves a trachyphonolitic magma (Monte Nuovo 1538 AD, D'Oriano et al. 2005; Piochi et al. 2005). PWW and Monte Nuovo eruptions were similar in that they both produced extremely diverse pyroclast types (D'Oriano et al. 2005). The Monte Nuovo



26 Page 18 of 24 Bull Volcanol (2017) 79:26

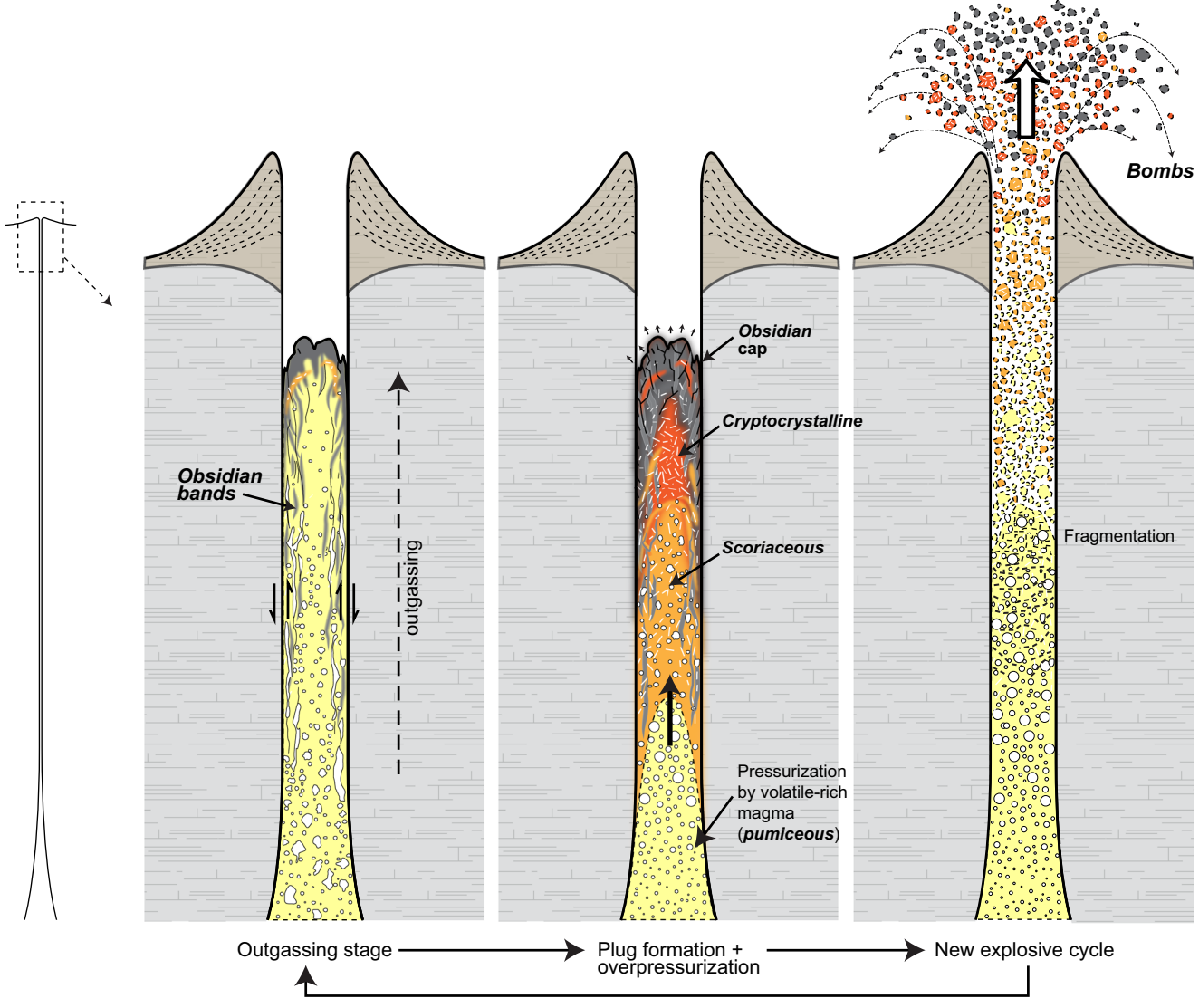


Fig. 12 Inferred explosion cycle at Pu u Wa awa a and "textural" profiles across the conduit. At the end of each explosion, residual magma is no longer highly overpressurized and ascends slower (*left*). Permeability development and bubble collapse produce magma, which is largely microlite and vesicle poor, that develops an obsidian cap at the top. Outgassing and bubble collapse may be enhanced towards the

conduit edges, resulting in banding. As the cap solidifies into a plug, completely or partially outgassed magma crystallizes (future "cryptocrystalline" and "scoriaceous" clasts, respectively) (center).  $\rm H_2O$ -rich magma repressurizes the system from below (later forming "pumiceous" clasts) up to plug disruption and explosion ( $\it right$ )

eruption differed in having emplaced large PDCs in addition to a few fallout phases and showing a clear compositional and eruptive style transition (phreatomagmatic to magmatic) from the lower to the upper members. Both PWW and Monte Nuovo eruptions, nonetheless, involved cyclic formation and destruction of conduit plugs.

# The influence of viscosity and melt water content on eruption style

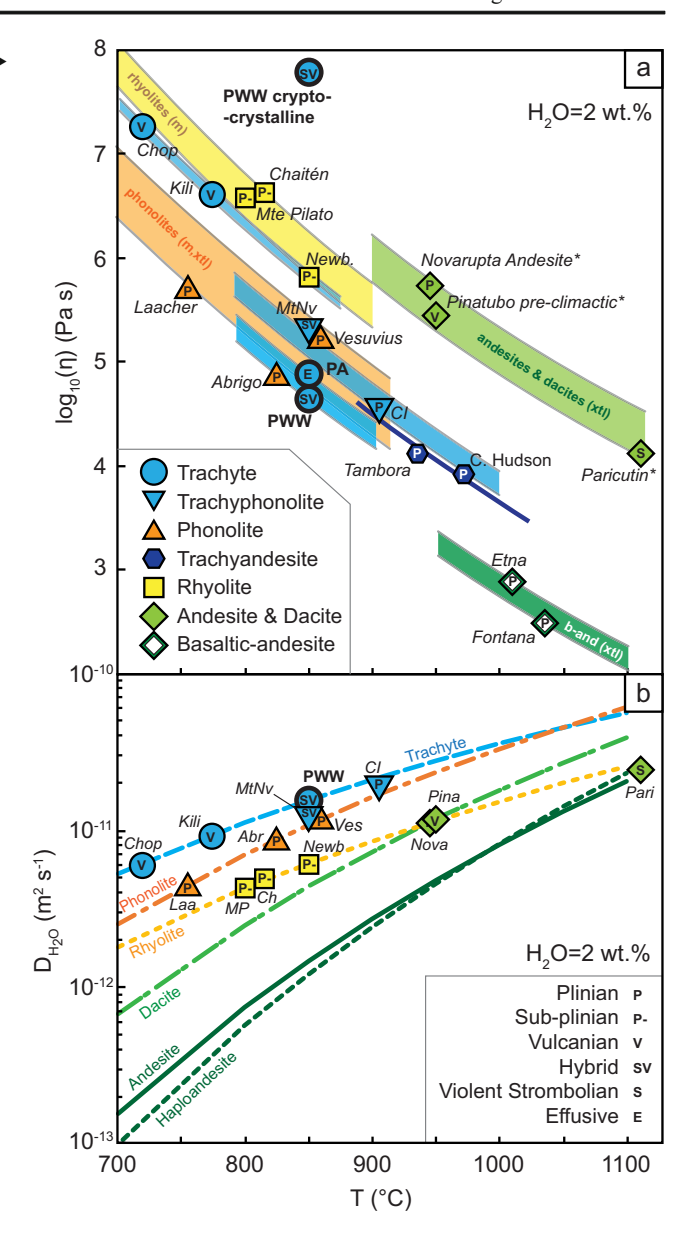
The inferred intermediate eruption dynamics between conebuilding violent Strombolian and Vulcanian at PWW may be related to the low viscosity associated with a fairly unusual trachyte composition. Compared to Monte Nuovo 1538 AD and other arc and rift trachytes that produced domes and/or large PDCs, the Pu'u Wa'awa'a trachyte is richer in alkalis, particularly in Na<sub>2</sub>O, slightly less aluminous, and less phenocryst-rich, resulting in lower melt viscosities. To provide a more general comparison, magma viscosities were calculated for other compositions spanning a range in eruption styles (violent Strombolian, Vulcanian, subplinian, and Plinian) and for which compositional, temperature, and textural (i.e., phenocryst content) constraints were available (c.f. Takeuchi 2011; Andujar and Scaillet 2012). For each eruption, melt viscosities were recalculated using the model of Giordano et al. (2008) and the crystal-bearing magma viscosities using



Bull Volcanol (2017) 79:26 Page 19 of 24 26

Fig. 13 a Bulk (melt + crystals) viscosity calculated for different types of intermediate to evolved magmas involved in several well-studied explosive eruptions, for H2O = 2 wt%. Viscosity of Pu'u Wa'awa'a and Pu'u Anahulu magmas are also reported, assuming a temperature T = 850 °C. Arrays show observed range in viscosity for "m" near melt-only (<5% vol. phenocrysts) and for "xtl" phenocryst-rich magmas. b Diffusivity of H2O in andesite, dacite, rhyolite, phonolite, and trachyte melts containing 2 wt% H<sub>2</sub>O. Eruptions examined in a are shown here assuming a unique composition for each magma type (i.e., all trachytes obey the same diffusivity model). Glass compositions and crystal content data: Rhyolites: Newberry 1300BP, Oregon (Gardner et al. 1998; Rust and Cashman 2007); Monte Pilato 776AD, Aeolian Islands (Gottsmann and Dingwell 2001; Davi et al. 2011); Chaiten 2008AD, Chile (Castro and Dingwell 2009). Dacites: Pinatubo\* 1991AD, Philippines (Pallister et al. 1996; Rutherford and Devine 1996); Novarupta 1912AD, Alaska (Hammer et al. 2002). Andesites: Paricutin\* 1943AD, Mexico (Pioli et al. 2008). Trachytes: Puy Chopine 9700BP and Kilian 9200BP, Chaîne des Puys (Martel et al. 2013); Pu'u Wa'awa'a and Pu'u Anahulu ~106-114 ka trachytes: This study, Trachyphonolites and trachyandesites: Campanian Ignimbrite 39ka, Italy (Polacci et al. 2001; Fowler et al. 2007); Monte Nuovo 1538AD, Italy (D'Oriano et al. 2005; Piochi et al. 2005); Tambora 1815AD, Indonesia (Self et al. 2004; Andujar and Scaillet 2012); Cerro Hudson 1991AD (Kratzmann et al. 2009). Phonolites: Vesuvius 79AD (Shea et al. 2012, 2014); Laacher See 12,900BP, Germany (Harms et al. 2004; Andujar and Scaillet 2012); Abrigo 190ka, Tenerife (Andujar et al. 2008, Takeuchi 2011). Diffusivity models: Rhyolites: Ni and Zhang (2008); Dacites: Ni et al. (2009); Andesite: Behrens et al. (2004); Haploandesite: Zhang and Ni (2010); Phonolites: Schmidt et al. (2013); Trachytes: Fanara et al. (2013)

Mader et al. (2013). To isolate the effects of composition and crystal content from water contents, all magmas were given a pre-eruptive H<sub>2</sub>O content of 2 wt%, assumed representative of a shallow magma close to eruption. Although the bubble content of a magma can affect its viscosity significantly (e.g., Llewellin and Manga 2005), we surmise that to a first order, all the magmas considered had negligible pre-eruptive vesicularities. A tentative temperature of 850 °C was chosen for PWW based on phase equilibria arguments (cf. next section). The pre-eruptive viscosity of the PWW trachyte ( $\sim 10^{4.6}$  Pa s) lies at the low end of the bounds defined by trachytes and phonolites on a viscosity vs. temperature plot (Fig. 13a). PWW is therefore unique in that unlike other trachytes (e.g., Giordano et al. 2004), its viscosity is lower than that of most phonolites. In the realm of alkalic magmas, only the viscosities of trachyandesites fall below values for PWW, but they were all likely hotter magmas. Eruptions that involved viscous domes and/or substantial Vulcanian activity (Chopine, Kilian, Novarupta, Pinatubo) involved magmas that were more viscous than PWW. Aside from differences in melt composition, the higher viscosity of these magmas is also associated with higher crystal content, particularly for the calc-alkaline examples. In contrast, the basaltic andesite magma from the endmember violent Strombolian eruption considered (Paricutin) has only a marginally lower viscosity than PWW. As suggested by Cashman and Sparks (2013), crystal content likely plays an important role in shifting eruption styles towards lower (Strombolian, violent Strombolian) or higher intensities



(Vulcanian). Subplinian eruptions involving crystal-poor rhyolites (Chaiten, Newberry, and Monte Pilato) all have significantly higher viscosities than PWW. The relatively low viscosity compared to other intermediate and evolved magmas worldwide may be one factor to explain why the PWW eruption did not reach the intensity of larger Vulcanian or subplinian eruptions. Instead, the resulting deposits possess transitional lithofacies and pyroclast characteristics between those of violent Strombolian and Vulcanian eruptions, with high explosion frequency and pulsatory behavior (e.g., Dominguez et al. 2016).

Viscosity is clearly not the only parameter that dictates eruption style, considering the various instances that attained Plinian intensities despite involving less viscous magmas (Fontana Lapilli, Etna 122 BC, Cerro Hudson 1991 AD, Tambora 1815 AD, Campanian Ignimbrite). Andujar and



26 Page 20 of 24 Bull Volcanol (2017) 79:26

Scaillet (2012) proposed that pre-eruptive H<sub>2</sub>O content at the storage level may exert the dominant control on the explosivity of phonolites and trachytes. The exact relationship between pre-eruptive H<sub>2</sub>O and explosivity is, however, still unclear because (1) the vast majority of studied phonolite and trachyte eruptions are explosive and the more effusive endmembers are underrepresented, and (2) there are clear outlier examples of eruptions involving magmas with very high initial H<sub>2</sub>O (e.g., Chaîne des Puys trachytes with ~8 wt% H<sub>2</sub>O, Martel et al. 2013) that produced Vulcanian eruptions much smaller in volume than Plinian eruptions involving magmas with lower inferred initial H<sub>2</sub>O (e.g., Campanian Ignimbrite with ~6 wt% H<sub>2</sub>O, Marianelli et al. 2006) associated with Plinian eruptions by two orders of magnitude larger in volume. Below, we discuss factors other than viscosity and initial H<sub>2</sub>O content, including the propensity of trachytes to degas and crystallize faster than other magmas.

### Trachyte: a "reactive" magma?

Within the realm of magmas at the end of their differentiation paths, alkalic magmas (phonolites and trachytes) differ notably in vesiculation and crystallization behavior compared to their calc-alkaline counterparts (dacites and rhyolites). Feldspar crystallizes faster in trachyte magma than in rhyodacites or rhyolites at similar P and T conditions (Arzilli and Carroll 2013). The tendency of trachytes to respond to perturbations (e.g., H<sub>2</sub>O degassing) by crystallizing rapidly is reflected in the extreme variability of microlite contents within the different textural end-members of the PWW pyroclasts. Most phenocryst-free rhyolites are comparatively sluggish and typically have low microlite abundances after eruption and quenching. For instance, rhyolite lava flows generally preserve a microlite-poor obsidian carapace (e.g., Fink 1983; Manley and Fink 1987), a feature that is absent from the thick, holocrystalline Pu'u Anahulu flow.

Experimental studies of vesiculation in phonolite and trachyte melts have also shown that they respond rapidly to decompression, and their vesicularity and  $H_2O$  content track values predicted at equilibrium more readily than rhyolites (Larsen and Gardner 2004; Larsen 2008; Mongrain et al. 2008; Shea et al. 2010b; Preuss et al. 2016).

The propensity of evolved alkalic magmas to crystallize or vesiculate more readily than their calc-alkalic counterparts is likely a consequence of faster H<sub>2</sub>O and crystal-forming cation diffusion (e.g., Behrens and Hahn 2009; Fanara et al. 2013), which control bubble/crystal nucleation and growth. Degassing kinetics are partly controlled by H<sub>2</sub>O diffusion in the melt, and existing studies have shown that water diffusivities are higher in trachytes than in other magmas (Fig. 13b). Thus, degassing may occur at faster rates in trachyte, maintaining lower levels of supersaturation and potentially conduit overpressure compared to dacites and rhyolites. On the other

hand, fast degassing kinetics coupled with relatively rapid crystallization rates in trachytes may favor formation of crystalline subregions and plugs within the conduit and the build-up of overpressure like at PWW or Monte Nuovo (e.g., D'Oriano et al. 2005). Notwithstanding, the emerging picture from experimental constraints on the intrinsic properties of trachyte magmas coupled with observations on the remarkable textural diversity of natural trachyte samples suggests that they are kinetically more "reactive" magmas compared to their less alkaline differentiated equivalents.

### The highly variable eruption styles of Hawaiian trachytes

The Pu'u Wa'awa'a cone, the Pu'u Anahulu flow, and the Hualālai ignimbrite sequence form the three principal trachyte eruptions now recognized on Hualālai volcano. These three distinct events ranging in eruption style from effusive (Pu'u Anahulu) to highly explosive (Hualālai ignimbrites) involved petrologically similar magmas (i.e., very few or no phenocrysts, groundmass of anorthoclase microlites/ microphenocrysts, magnetite, and apatite) despite the slight differences in bulk compositions. Obsidian, scoriaceous, and cryptocrystalline clasts are also found within the coarser units of the Hualālai ignimbrites (Shea and Owen 2016), suggesting that conduit obstruction and formation of dense plugs may have played some role as well. In contrast to Pu'u Wa'awa'a, however, the eruption column that produced the ignimbrites was likely significantly larger and never fully stable.

Based on the compositional similarity and the comparable mineral assemblages in the groundmass, we infer that the differences in eruption styles did not result from fundamental differences in magma characteristics in the storage area (i.e., temperature, viscosity, water saturation). Although no phase equilibria experiments exist for Hawaiian trachyte compositions, a MELTS-generated P-T mineral equilibria diagram tentatively indicates temperatures of ~800-850 °C for all three trachytes (Fig. A8 in the Supplementary Material). Storage pressures cannot be constrained because similar phases crystallize over a wide range in pressure. The contrasts in eruption dynamics may therefore be related to (1) varying storage depths and hence ascent times or (2) other external factors that allowed the different magmas to outgas more or less easily. External factors could include differing vent dimensions or geometries (larger or extended/elongate vent may facilitate magma outgassing compared to a smaller point source) or differences in the geometry of the feeder system (e.g., Wilson et al. 1980; Legros et al. 2000). The magma that fed the voluminous Pu'u Anahulu flow may therefore have resided deeper than those that produced the Pu'u Wa'awa'a cone or Hualālai ignimbrite, giving enough time for degassing and outgassing to progress under near equilibrium conditions during ascent. Alternatively, Pu'u Anahulu may have been fed by



Bull Volcanol (2017) 79:26 Page 21 of 24 26

a larger/more extended fracture system and/or erupted along a fissure. The latter possibility would also explain why the PA feeder vent system may have been topographically subdued enough to be covered by subsequent basalt flows, whereas the more central PWW vent was more prominent and largely preserved from burial.

### **Conclusions**

The field, textural, and chemical investigation of Pu'u Wa'awa'a and Pu'u Anahulu erupted during the ~110-ka period of Hualālai volcano provides several key pieces of information to understand trachyte volcanism in Hawai'i:

- In contrast to what has been assumed previously, the Pu'u Wa'awa'a cone and the Pu'u Anahulu flow were likely erupted during two separate events. A third eruption produced the Hualālai ignimbrites, which largely covered the Pu'u Anahulu flow. The lack of Pu'u Wa'awa'a tephra on top of or below the ignimbrites and the slight differences in composition between the three eruption products altogether confirm that various trachyte reservoirs probably existed on Hualālai ~110 ka. Detailed regional geophysical surveys (gravity, seismic) are needed to constrain the distribution of the PWW tephra under the recent basaltic lava flow cover. Modern dating techniques (Ar<sup>40</sup>/Ar<sup>39</sup>) could also aid in testing whether these three events (in addition to the trachytes found at Waha Pele and Huehue) were separated in time.
- The PWW cone was built during an eruption transitional in style between violent Strombolian and Vulcanian. The deposit architecture has characteristics similar to those of large basaltic scoria cones (e.g., heavy proximal remobilization), while pyroclast textures show evidence for conduit plug formation. The Hualālai ignimbrites studied previously were likely produced during a larger, higher intensity explosive eruption while the large-volume Pu'u Anahulu flow was erupted effusively. Therefore, trachytes erupted at Hualālai provide evidence for important contrasts in eruption dynamics that are unlikely to have been related to differences in intrinsic magmatic parameters but rather associated with differing conditions of magma ascent. Further investigations of vesicle and microlite textures (e.g., number density, size distributions) may help estimate variations in ascent and/or exsolution rates.
- The astonishing variety of pyroclast morphologies, colors, textures, and interstitial glass compositions at Pu'u Wa'awa'a can be related entirely to the extent of magma degassing and outgassing within the conduit.

- Post-eruptive meteoric rehydration appears to have controlled  $\rm H_2O$  concentrations in pyroclasts with >40% vol. porosity (likely a consequence of the high vesicle connectivity), meaning that only clasts with lower vesicularity can be used to make inferences on primary magma water contents and degassing.
- Trachytes increasingly appear as kinetically faster magmas compared to rhyolites or even dacites with respect to crystallization and, potentially, degassing. The combination of low viscosity with the propensity for the PWW trachyte to degas and crystallize microlites rapidly probably led to the hybrid eruption style between violent Strombolian and Vulcanian. Future experiments investigating vesiculation and/or crystallization of trachytes under decompression may help determine whether faster H<sub>2</sub>O and feldspar-forming cation mobilities in the melt can explain those differences adequately.

**Acknowledgements** This study was funded by NSF EAR Grant 1250366 to TS and JL. Dave Clague is thanked for the many helpful discussions on Hualālai trachytes and Pu'u Wa'awa a. Field work was made possible by HETF, DOFAW. Help in the field by Jacqui Owen was also greatly appreciated. The detailed, constructive comments of Kathy Cashman, Lucia Gurioli, and an anonymous reviewer enhanced the manuscript significantly.

### References

- Adams NK, Houghton BF, Fagents SA, Hildreth W (2006) The transition from explosive to effusive eruptive regime: the example of the 1912 Novarupta eruption. Alaska Geol Soc Am Bull 118:620–634
- Alvarado GE, Pérez W, Vogel TA, Gröger H, Patiño L (2011) The Cerro Chopo basaltic cone (Costa Rica): an unusual completely reversed graded pyroclastic cone with abundant low vesiculated cannonball juvenile fragments. J Volcanol Geotherm Res 201:163–177
- Andronico D, Cristaldi A, Del Carlo P, Taddeucci J (2009) Shifting styles of basaltic explosive activity during the 2002–03 eruption of Mt. Etna, Italy. J Volcanol Geotherm Res 180:110–122
- Andujar J, Scaillet B (2012) Relationships between pre-eruptive conditions and eruptive styles of phonolite—trachyte magmas. Lithos 152: 122–131
- Andújar J, Costa F, Martí J, Wolff JA, Carroll MR (2008) Experimental constraints on pre-eruptive conditions of phonolitic magma from the caldera-forming El Abrigo eruption, Tenerife (canary islands). Chem Geol 257:173–191
- Arzilli F, Carroll MR (2013) Crystallization kinetics of alkali feldspars in cooling and decompression-induced crystallization experiments in trachytic melt. Contrib Mineral Petrol 166:1011–1027
- Barberi F, Innocenti F, Lirer L, Munno R, Pescatore T, Santacroce R (1978) The Campanian Ignimbrite: a major prehistoric eruption in the Neapolitan area (Italy). Bull Volcanol 41:10–31
- Behrens H, Hahn M (2009) Trace element diffusion and viscous flow in potassium-rich trachytic and phonolitic melts. Chem Geol 259:63–
- Belousov A, Voight B, Belousova M (2007) Directed blasts and blastgenerated pyroclastic density currents: a comparison of the Bezymianny 1956, Mount St Helens 1980, and Soufriere Hills, Montserrat 1997 eruptions and deposits. Bull Volcanol 69:701–740



26 Page 22 of 24 Bull Volcanol (2017) 79:26

Behrens H, Zhang Y, Xu Z (2004) H<sub>2</sub>O diffusion in dacitic and andesitic melts. Geochim Cosmochim Acta 68:5139–5150

- Bernard B, Hidalgo S, Robin C, Beate B, Quijozaca J (2014) The 3640–3510 BC rhyodacite eruption of Chachimbiro compound volcano, Ecuador, a violent directed blast produced by a satellite dome. Bull Volcanol 76:1–20
- Boivin P, Besson J-C, Briot D, Camus G, De Goër HA, Gourgaud A, Labazuy P, Langlois E, Larouzière F-D, Livet M, Mergoil J, Miallier D, Morel J-M, Vernet G, Vincent PM (2009) Volcanologie de la Chaîne des Puys, Massif Central Français, 5th edn. Parc Naturel Régional des Volcans d'Auvergne Clermont-Ferrand, Geological Map
- Branney MJ, Kokelaar BP (2002) Pyroclastic density currents and the sedimentation of ignimbrites. Geol Soc Lond Mem 27
- Brugger CR, Hammer JE (2010) Crystallization kinetics in continuous decompression experiments: implications for interpreting natural magma ascent processes. J Petrol 51:1941–1965
- Cabrera A, Weinberg RF, Wright H, Zlotnik S, Cas RAF (2011) Melt fracturing and healing: a mechanism for degassing and origin of silicic obsidian. Geology 39:67–70
- Cagnoli B, Romano GP, Ventura G (2015) Shaking of pyroclastic cones and the formation of granular flows on their flanks: results from laboratory experiments. J Volcanol Geotherm Res 306:83–89
- Cashman KV, Sparks RSJ (2013) How volcanoes work: a 25 year perspective. Geol Soc Am Bull 125:664–690
- Castro JM, Dingwell DB (2009) Rapid ascent of rhyolitic magma at Chaitén volcano, Chile. Nature 461:780–783
- Church BN, Johnson WN (1980) Calculation of the refractive index of silicate glasses from chemical composition. Geol Soc Am Bull 91: 619–625
- Cimarelli C, Di Traglia F, Taddeucci J (2010) Basaltic scoria textures from a zoned conduit as precursors to violent Strombolian activity. Geology 38:439–442
- Clague DA, Jackson ED, Wright TL (1980) Petrology of Hualālai volcano, Hawai'i: implications for mantle composition. Bull Volcanol 43: 641–656.
- Clague DA (1987) Hawaiian xenolith population, magma supply rates, and development of magma chambers. Bull Volcanol 49:577–587
- Clague DA, Bohrson WA (1991) Origin of xenoliths in the trachyte at Puu Waawaa, Hualalai Volcano, Hawaii. Contrib Mineral Petrol 108:439–452
- Clarke AB, Stephens S, Teasdale R, Sparks RSJ, Diller K (2007) Petrologic constraints on the decompression history of magma prior to Vulcanian explosions at the Soufriere Hills volcano, Montserrat. J Volcanol Geotherm Res 161:261–274
- Clarke AB, Esposti Ongaro T, Belousov A (2015) Vulcanian eruptions. In: Sigurdsson H, Houghton B, McNutt S, Rymer H, Stix J (Eds), Encyclopedia of Volcanoes. p. 505–518
- Cross W (1904) An occurrence of trachyte on the island of Hawaii. J Geol 12:510–523
- Colombier M, Gurioli L, Druitt TH, Shea T, Boivin P, Miallier D, Cluzel N (2017) Textural evolution of magma during the 9.4-ka trachytic explosive eruption at Kilian Volcano, Chaine des Puys, France, Bulletin of Volcanology, 79:17
- Cousens BL, Clague DA, Sharp WD (2003) Chronology, chemistry, and origin of trachytes from Hualalai volcano, Hawaii. Geochem Geophys Geosyst 4(9)
- de Silva S, Lindsay JM (2015) Primary volcanic landforms. In: Sigurdsson H, Houghton B, McNutt S, Rymer H, Stix J (Eds), Encyclopedia of Volcanoes. p. 273–297
- Davi M, De Rosa R, Donato P, Sulpizio R (2011) The Lami pyroclastic succession (Lipari, Aeolian Islands): a clue for unravelling the eruptive dynamics of the Monte Pilato rhyolitic pumice cone. J Volcanol Geotherm Res 201:285–300
- D'Oriano C, Poggianti E, Bertagnini A, Cioni R, Landi P, Polacci M, Rosi M (2005) Changes in eruptive style during the A.D. 1538 Monte

- Nuovo eruption (Phlegrean Fields, Italy): the role of syn-eruptive crystallization. Bull Volcanol 67:601–621
- Di Genova D, Hess K-U, Oryaelle Chevrel M, Dingwell DB (2016) Models for the estimation of Fe<sup>3+</sup>/Fe<sub>tot</sub> ratio in terrestrial and extraterrestrial alkali- and iron-rich silicate glasses using Raman spectroscopy. Am Mineral 101:943–952
- Di Matteo V, Carroll MR, Behrens H, Vetere F, Brooker R (2004) Water solubility in trachytic melts. Chem Geol 213:187–196
- Di Muro A, Métrich N, Mercier M, Giordano D, Massare D, Montagnac G (2009) Micro-Raman determination of iron redox state in dry natural glasses: application to peralkaline rhyolites and basalts. Chem Geol 259:78–88
- Di Traglia F, Cimarelli C, De Rita D, Gimeno Torrente D (2009) Changing eruptive styles in basaltic explosive volcanism: examples from Croscat complex scoria cone, Garrotxa Volcanic Field (NE Iberian Peninsula). J Volcanol Geotherm Res 180:89–109
- Dominguez L, Pioli L, Bonadonna C, Connor CB, Andronico D, Harris AJL, Ripepe M (2016) Quantifying unsteadiness and dynamics of pulsatory volcanic activity. Earth Planet Sci Lett 444:160–168
- Druitt TH, Young SR, Baptie BJ, Bonadonna C, Calder ES, Clarke AB, Cole PD, Harford CL, Herd RA, Lockett R, Ryan G, Voight B (2002) Episodes of cyclic Vulcanian explosive activity with fountain collapse at Soufrière Hills volcano, Montserrat. In: Druitt TH, Kokelaar BP (eds), the eruption of Soufrière Hills volcano, Montserrat, from 1995 to 1999. Geol Soc London Mem 21:281–306
- Edmonds M, Oppenheimer C, Pyle DM, Herd RA, Thompson G (2003) SO<sub>2</sub> emissions from Soufriere Hills volcano and their relationship to conduit permeability, hydrothermal interactions and degassing regime. J Volcanol Geotherm Res 124:23–43
- Eichelberger JC, Carrigan CR, Westrich HR, Price RH (1986) Nonexplosive silicic volcanism. Nature 323:598–602
- Fabbrizio A, Carroll MR (2008) Experimental constraints on the differentiation process and pre-eruptive conditions in the magmatic system of Phlegraean Fields (Naples, Italy). J Volcanol Geoth Res 171: 88–102
- Fanara S, Behrens H, Zhang Y (2013) Water diffusion in potassium-rich phonolitic and trachytic melts. Chem Geol 346:149–161
- Fink JH (1983) Structure and emplacement of a rhyolitic obsidian flow: Little Glass Mountain, Medicine Lake Highland, northern California. Geol Soc Am Bull 94:362–380
- Formenti Y, Druitt TH (2003) Vesicle connectivity in pyroclasts and implications for the fluidization of fountain-collapse pyroclastic flows, Montserrat (West Indies). Earth Planet Sci Lett 214:561–574
- Fowler SJ, Spera F, Bohrson W, Belkin HE, De Vivo B (2007) Phase equilibria constraints on the chemical and physical evolution of the campanian ignimbrite. J Petrol 48:459–493
- Freundt A, Schmincke H-U (1995) Petrogenesis of rhyolite trachytebasalt composite ignimbrite P1, Gran Canaria, Canary Islands. J Geophys Res 100:455–474
- Frey FA, Wise WS, Garcia MO, West H, Kwon S-T, Kennedy A (1990) Evolution of Mauna Kea volcano, Hawaii: petrologic and geochemical constraints on postshield volcanism. J Geophys Res 95:1271–1300
- Gardner JE, Carey S, Sigurdsson H (1998) Plinian eruptions at Glacier Peak and Newberry volcanoes, United States: implications for volcanic hazards in the Cascade Range. Geol Soc Amer Bull 110:173– 187
- Geschwind C, Rutherford MJ (1995) Crystallization of microlites during magma ascent: the fluid mechanics of recent eruptions at Mount St. Helens. Bull Volcanol 57:356–370
- Giachetti T, Druitt TH, Burgisser A, Arbaret A, Galven C (2010) Bubble nucleation, growth, and coalescence during the 1997 Vulcanian explosions of Soufriere Hills volcano, Montserrat. J Volcanol Geotherm Res 193:215–231
- Giachetti T, Gonnermann HM (2013) Water in volcanic pyroclast: rehydration or incomplete degassing? Earth Planet Sci Lett 369:317–332



Bull Volcanol (2017) 79:26 Page 23 of 24 26

- Giachetti T, Gonnermann H, Gardner J, Shea T, Gouldstone A (2015) Discriminating secondary from magmatic water in rhyolitic matrixglass of volcanic pyroclasts using thermogravimetric analysis. Geochim Cosmochim Acta 148:457–476
- Giordano D, Romano C, Papale P, Dingwell DB (2004) The viscosity of trachytes, and comparison with basalts, phonolites, and rhyolites. Chem Geol 213:49–61
- Giordano D, Russell JK, Dingwell DB (2008) Viscosity of magmatic liquids: a model. Earth Planet Sci Lett 271:123–134
- Gottsmann J, Dingwell DB (2001) The cooling of frontal flow ramps: a calorimetric study on the Rocche Rosse rhyolite flow, Lipari, Aeolian Islands, Italy. Terra Nov. 13:157–164
- Gurioli L, Colò L, Bollasina AJ, Harris AJL, Whittington A, Ripepe M (2014) Dynamics of strombolian explosions: inferences from inferences from field and laboratory studies of erupted bombs from Stromboli volcano. J Geophys Res 119:319–345
- Hammer JE, Cashman KV, Hoblitt RP, Newman S (1999) Degassing and microlite crystallization during pre-climactic events of the 1991 eruption of Mt. Pinatubo, the Philippines. Bull Volcanol 60:355–380
- Hammer JE, Rutherford MJ, Hildreth W (2002) Magma storage prior to the 1912 eruption at Novarupta, Alaska. Contrib Mineral Petrol 144: 144–162
- Hammer JE, Coombs M, Shamberger PJ, Kimura J (2006) Submarine sliver in North Kona: a window into the early magmatic and growth history of Hualalai volcano, Hawaii. J Volcanol Geotherm Res 151: 157–188
- Hanano D, Weis D, Scoates JS, Aciego S, DePaolo DJ (2010) Horizontal and vertical zoning of heterogeneities in the Hawaiian mantle plume from the geochemistry of consecutive postshield volcano pairs: Kohala-Mahukona and Mauna Kea-Hualalai. Geochem Geophys Geosyst 11:Q01004
- Harms E, Gardner JE, Schmincke H-U (2004) Phase equilibria of the lower Laacher See Tephra (East Eifel, Germany): constraints on pre-eruptive storage conditions of a phonolitic magma reservoir. J Volcanol Geotherm Res 134:135–148
- Hoblitt RP, Harmon RS (1993) Bimodal density distribution of cryptodome dacite from the 1980 eruption of Mt. St. Helens, Washington. Bull Volcanol 55:421–437
- Kauahikaua J, Hildenbrand T, Webring M (2000) Deep magmatic structures of Hawaiian volcanoes, imaged by three dimensional gravity models. Geology 28:883–886
- King BC, Chapman GR, Robson DA, McConnell RB (1972) Volcanism of the Kenya Rift Valley. Phil Trans Roy Soc London A 271:185– 208
- Klug C, Cashman KV (1994) Vesiculation of May 18, 1980, Mount St. Helens magma. Geology 22:468–472
- Kratzmann DJ, Carey S, Scasso R, Naranjo JA (2009) Compositional variations and magma mixing in the 1991 eruptions of Hudson volcano, Chile. Bull Volcanol 71:419–439
- Larsen JF, Gardner JE (2004) Experimental study of water degassing from phonolite melts: implications for volatile oversaturation during magmatic ascent. J Volcanol Geotherm Res 134:109–124
- Larsen JF (2008) Heterogeneous bubble nucleation and disequilibrium H<sub>2</sub>O exsolution in Vesuvius K-phonolite melts. J Volcanol Geotherm Res 275:278–288
- Lautze N, Houghton BF (2007) Linking explosion intensity and magma rheology during 2002 at Stromboli volcano. Bull Volcanol 69:445– 460
- Lavallée Y, Benson PM, Heap MJ, Hess K-U, Flaws A, Schillinger B, Meredith PG, Dingwell DB (2013) Reconstructing magma failure and the degassing network of dome-building eruptions. Geology 41: 515–518
- Leduc L, Gurioli L, Harris A et al (2015) Types and mechanisms of Strombolian explosions: characterization of a gas-dominated explosion at Stromboli. Bull Volcanol 77(8)

- Legros F, Kelfoun K, Marti J (2000) The influence of conduit geometry on the dynamics of caldera-forming eruptions. Earth Planet Sci Lett 179:53–61
- Le Losq C, Neuville DR, Moretti R, Roux J (2012) Determination of water content in silicate glasses using Raman spectrometry: implications for the study of explosive volcanism. Am Mineral 97:779–790
- Llewellin EW, Manga M (2005) Bubble suspension rheology and implications for conduit flow. J Volcanol Geotherm Res 143:205–217
- Lipman PW, Coombs ML (2006) Submarine slumping on the north Kona flank of Hualālai volcano (Hawaii) during tholeiitic shield-stage volcanism. J Volcanol Geotherm Res 151:189–216
- Macdonald GA (1968) Composition and origin of Hawaiian lavas. In: Hay, R. L. & Anderson, C. A. (eds) Studies in Volcanology: A Memoir in Honour of Howel Williams. Geol Soc Am Mem 116: 477–522
- Mader HM, Llewellin EW, Mueller SP (2013) The rheology of two-phase magmas: a review and analysis. J Volcanol Geotherm Res 257:1–51
- Manley CR, Fink JH (1987) Internal textures of rhyolite flows as revealed by research drilling. Geology 15:549–552
- Marianelli P, Sbrana A, Proto M (2006) Magma chamber of the Campi Flegrei supervolcano at the time of eruption of the Campanian Ignimbrite. Geology 34:937–940
- Martel C, Schmidt BC (2003) Decompression experiments as an insight into ascent rates of silicic magmas. Contrib Mineral Petrol 144:397–415
- Martel C, Champallier R, Prouteau G, Pichavant M, Arbaret L, Balcone-Boissard H, Boudon G, Boivin P, Bourdier JL, Scaillet B (2013)
   Trachyte phase relations and implication for magma storage conditions in the Chaîne des Puys (French Massif Central). J Petrol 54: 1071–1107
- Miallier D, Boivin P, Deniel C, Gourgaud A, Lanos P, Sforna M, Pilleyre T (2010) The ultimate summit eruption of Puy de Dôme volcano (Chaine des Puys, French Massif Central) about 10,700 years ago. Comptes Rendus Géosciences 342:847–854
- Mongrain J, Larsen JF, King PL (2008) Rapid H<sub>2</sub>O exsolution, gas loss, and bubble collapse observed experimentally in K-phonolite melts. J Volcanol Geotherm Res 173:178–184
- Moore JG, Clague DA (1992) Volcano growth and evolution of the island of Hawaii. Geol Soc Am Bull 104:1471–1484
- Moore RB, Clague DA, Rubin M, Bohrson WA (1987) Hualalai volcano: a preliminary summary of geologic, petrologic, and geophysical data, in Volcanism in Hawaii, edited by RW Decker, TL Wright, and PH Stauffer, USGS Prof Pap 1350:571–585
- Morgan GB, London D (1996) Optimizing the electron microprobe analysis of hydrous alkali aluminosilicate glasses. Am Mineral 81:1176–1185
- Neill OK, Hammer JE, Izbekov P, Belousova MG, Belousov AB, Clarke AB, Voight B (2010) Influence of pre-eruptive degassing and crystallization on the juvenile products of laterally directed volcanic explosions. J Volcanol Geotherm Res 198:264–274
- Ni H, Zhang Y (2008) H<sub>2</sub>O diffusion models in rhyolitic melt with new high pressure data. Chem Geol 250:68–78
- Ni H, Behrens H, Zhang Y (2009) Water diffusion in dacitic melt. Geochim Cosmochim Acta 73:3642–3655
- Nichols ARL, Wysoczanski RJ (2007) Using micro-FTIR spectroscopy to measure volatile contents in small and unexposed inclusions hosted in olivine crystals. Chem Geol 242:371–384
- Pallister JS, Hoblitt RP, Meeker GP, Knight RJ, Siems DF (1996) Magma mixing at Mount Pinatubo: petrographic and chemical evidence from the 1991 deposits. In: Newhall CG, Punongbayan RS (eds) Fire and mud: eruptions and lahars of mount Pinatubo, Philippines. Univ. of Wash. Press, Seattle, pp 687–732
- Paulick H, Franz G (1997) The color of pumice: case study on trachytic fall deposit, Meidob volcanic field, Sudan. Bull Volcanol 59:171– 185



26 Page 24 of 24 Bull Volcanol (2017) 79:26

Pecerillo A (2005) Plio-quaternary volcanism in Italy. Springer-Verlag Berlin Heidelberg 365p

- Piochi M, Mastrolorenzo G, Pappalardo L (2005) Magma ascent and eruptive processes from textural and compositional features of Monte Nuovo pyroclastic products, Campi Flegrei, Italy. Bull Volcanol 67:663–678
- Pioli L, Erlund E, Johnson E, Cashman K, Wallace P, Rosi M, Delgado Granados H (2008) Explosive dynamics of violent Strombolian eruptions: the eruption of Parícutin volcano 1943–1952 (Mexico). Earth Planet Sci Lett 271:359–368
- Polacci M, Papale P, Rosi M (2001) Textural heterogeneities in pumices from the climactic eruption of Mount Pinatubo, 15 June 1991, and implications for magma ascent dynamics. Bull Volcanol 63:83–97
- Polacci M, Pioli L, Rosi M (2003) The Plinian phase of the Campanian Ignimbrite eruption (Phlegrean Fields, Italy): evidence from density measurements and textural characterization of pumice. Bull Volcanol 65:418–432
- Polacci M, Bouvet de Maisonneuve C, Giordano D, Piochi M, Mancini L, Degruyter W, Bachmann O (2014) Permeability measurements of Campi Flegrei pyroclastic products: an example from the Campanian Ignimbrite and Monte Nuevo eruptions. J Volcano Geotherm Res 272:16–22
- Preuss O, Marxer H, Ulmer S, Wolf J, Nowak M (2016) Degassing of hydrous trachytic Campi Flegrei and phonolitic Vesuvius melts: experimental limitations and chances to study homogeneous bubble nucleation. Am Min 101:859–875
- Rosi M, Landi P, Polacci M, Di Muro A, Zandomeneghi D (2004) Role of conduit shear on ascent of the crystal-rich magma feeding the 800year-BP Plinian eruption of Quilotoa volcano (Ecuador). Bull Volcanol 66:307–321
- Rust AC, Cashman KV (2007) Multiple origins of obsidian pyroclasts and implications for changes in the dynamics of the 1300 B.P. eruption of New-berry Volcano, USA. Bull Volcanol 69:825–845
- Rutherford MJ, Devine JD (1996) Pre-eruption pressure-temperature conditions and volatiles in the 1991 dacitic magma of Mount Pinatubo.
  In: Newhall C, Punongbayan R (eds) Fire and mud: eruptions and lahars of Mount Pinatubo, Philippines. Univ. of Wash. Press, Seattle, pp 751–766
- Schipper CI, Castro JM, Tuffen H, James MR, How P (2013) Shallow vent architecture during hybrid explosive–effusive activity at Cordón Caulle (Chile, 2011–12): evidence from direct observations and pyroclast textures. J Volcanol Geotherm Res 262:25–37
- Schmidt BC, Blum-Oeste N, Flagmeier J (2013) Water diffusion in phonolite melts. Geochim Cosmochim Acta 107:220–230
- Schmincke H-U, Park C, Harms E (1999) Evolution and environmental impacts of the eruption of Laacher See Volcano (Germany) 12,900 a BP. Quat Int 61:61–72
- Self S, Gertisser R, Thordarson T, Rampino MR, Wolff JA (2004) Magma volume, volatile emissions, and stratospheric aerosols from the 1815 eruption of Tambora. Geophys Res Lett 31:L20608
- Shamberger PJ, Hammer JE (2006) Leucocratic and gabbroic xenoliths from Hualalai volcano, Hawaii. J Petrol 47:1785–1808
- Shea T, Owen J (2016) Discovery of a trachyte ignimbrite sequence at Hualālai, Hawaii. Bull Volcanol 78:34
- Shea T, Houghton BF, Gurioli L, Cashman KV, Hammer JE, Hobden B (2010a) Textural studies of vesicles in volcanic rocks: an integrated methodology. J Volcanol Geotherm Res 190:271–289

- Shea T, Gurioli L, Larsen JF, Houghton BF, Hammer JE, Cashman KV (2010b) Linking experimental and natural vesicle textures in Vesuvius 79 AD white pumice. J Volcanol Geotherm Res 192:69–84
- Shea T, Gurioli L, Houghton BF (2012) Transitions between fall phases and pyroclastic density currents during the AD 79 eruption at Vesuvius: building a transient conduit model from the textural and volatile record. Bull Volcanol 74:2363–2381
- Shea T, Hellebrand E, Gurioli L, Tuffen H (2014) Conduit- to localizedscale degassing during Plinian eruptions: insights from major element and volatile (Cl and H<sub>2</sub>O) analyses within AD79 Vesuvius pumices. J Petrol 55:315–344
- Sherrod DR, Murai T, Tagami T (2007a) New K–Ar ages for calculating end-of-shield extrusion rates at West Maui volcano, Hawaiian island chain. Bull Volcanol 69:627–642
- Sherrod DR, Sinton JM, Watkins SE, Brunt KM (2007b) Geologic map of the state of Hawai'i. USGS Open File Report:2007–1089
- Sigurdsson H, Cornell W, Carey S (1990) Influence of magma withdrawal on compositional gradients during the AD 79 Vesuvius eruption. Nature 345:519–521
- Sinton JM, Grönvold K, Sæmundsson K (2005) Postglacial eruptive history of the Western Volcanic Zone, Iceland. Geochem Geophys Geosyst 6:Q12009
- Spengler SR, Garcia MO (1988) Geochemistry of the Hawi lavas, Kohala volcano, Hawaii. Contrib Mineral Petrol 99:90–104
- Steams HT, Macdonald GA (1942) Geology and groundwater resources of the island of Maui, Hawaii. Hawaii Div Hydrography Bull 7
- Stearns HT, Macdonald GA (1946) Geology and groundwater resources of the island of Hawaii. Hawaii Div Hydrography Bull 7:344
- Takeuchi S (2011) Pre-eruptive magma viscosity: an important measure of magma eruptibility. J Geophys Res 116:B10201
- Valentine GA, Krier D, Perry FV, Heiken G (2005) Scoria cone construction mechanisms, Lathrop Wells volcano, southern Nevada, USA. Geology 33:629–632
- Van der Zander I, Sinton JM, Mahoney JJ (2010) Late shield-stage silicic magmatism at Wai'anae volcano: evidence for hydrous crustal melting in Hawaiian volcanoes. J Pet 51:671–701
- Velde D (1978) An aenigmatite-richterite-olivine trachyte from Puu Koae, West Maui, Hawaii. Am Mineral 63:771–778
- Wilson L, Sparks RSJ, Walker GPL (1980) Explosive volcanic eruptions—IV. The control of magma properties and conduit geometry on eruption column behavior. Geophys J Int 63:117–148
- Whittington A, Richet P, Linard Y, Holtz F (2001) The viscosity of hydrous phonolites and trachytes. Chem Geol 174:209–223
- Wolfe EW, Morris J (1996) Geologic map of the island of Hawaii. USGS Map I-2524-A
- Wright HMN, Cashman KV, Rosi M, Cioni R (2007) Breadcrust bombs as indicators of Vulcanian eruption dynamics at Guagua Pichincha volcano, Ecuador. Bull Volcanol 69:281–300
- Wright HMN, Folkes CB, Cas RAF, Cashman KV (2011) Heterogeneous pumice populations in the 2.08-Ma Cerro Galan ignimbrite: implications for magma recharge and ascent preceding a large-volume silicic eruption. Bull Volcanol 73:1513–1533
- Závada P, Schulmann K, Lexa O, Hrouda F, Haloda J, Týcová P (2009) The mechanism of flow and fabric development in mechanically anisotropic trachyte lava. J Struct Geol 31:1295–1307
- Zhang Y, Ni H (2010) Diffusion of H, C, and O components in silicate melts. Rev Mineral Geochem 72:171–225

